Article

Rational Design of a Chromo- and Fluorogenic Hybrid Chemosensor Material for the Detection of Long-Chain Carboxylates

Ana B. Descalzo, Knut Rurack, Hardy Weisshoff, Ramn Martnez-Mez, M. Dolores Marcos, Pedro Amors, Katrin Hoffmann, and Juan Soto

J. Am. Chem. Soc., **2005**, 127 (1), 184-200• DOI: 10.1021/ja045683n • Publication Date (Web): 07 December 2004

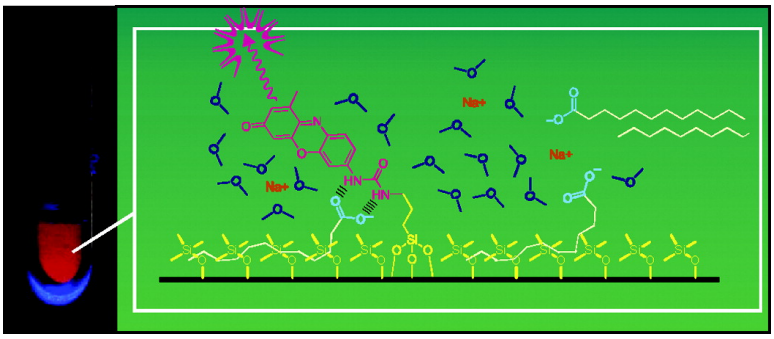

More About This Article

Additional resources and features associated with this article are available within the HTML version:

- Supporting Information
- Links to the 35 articles that cite this article, as of the time of this article download
- Access to high resolution figures
- Links to articles and content related to this article
- Copyright permission to reproduce figures and/or text from this article

View the Full Text HTML

J|A|C|S
ARTICLES
Published on Web 12/07/2004

Rational Design of a Chromo- and Fluorogenic Hybrid Chemosensor Material for the Detection of Long-Chain Carboxylates

Ana B. Descalzo,[†] Knut Rurack,*[,‡] Hardy Weisshoff,[‡,||] Ramón Martínez-Máñez,*[,†] M. Dolores Marcos,[†] Pedro Amorós,[§] Katrin Hoffmann,[‡] and Juan Soto[†]

Contribution from the Centro de Investigación en Química Molecular Aplicada, Departamento de Química, Universidad Politécnica de Valencia, Camino de Vera s/n, E-46071 Valencia, Spain, Div. I.3, Bundesanstalt für Materialforschung und -prüfung (BAM), Richard-Willstätter-Strasse 11, D-12489 Berlin, Germany, and Institut de Ciència dels Materials (ICMUV), Universitat de València, P.O. Box 2085, E-46071 València, Spain

Received July 19, 2004; E-mail: knut.rurack@bam.de; rmaez@qim.upv.es

Abstract: A strategy for the rational design of a new optical sensor material for the selective recognition of long-chain carboxylates in water is presented. The approach relies on the combination of structure−property relationships to single out the optimal molecular sensor unit and the tuning of the sensing characteristics of an inorganic support material. A spacer-substituted 7-urea-phenoxazin-3-one was employed as the signaling moiety and a mesoporous trimethylsilylated UVM-7 (MCM-41 type) material served as the solid support. The sensor material shows the advantageous features of both modules that is absorption and emission in the visible spectral range, a fluorescence red-shift and enhancement upon analyte coordination, and the amplification of noncovalent (binding) and hydrogen-bonding (recognition) interactions in the detection event. Besides these basic results that are related to the design and performance of the sensor material, the paper discusses general aspects of amido-substituted phenoxazinone photophysics and addresses some general features of molecular anion recognition chemistry in aqueous vs nonaqueous media, utilizing steady-state and time-resolved optical as well as NMR spectroscopies. Detailed studies on potentially competing biochemical species and a first access to the schematic model of the response of the sensor material as obtained by a combination of fluorescence lifetime distribution analysis and Langmuir-type fitting of the gross binding constants complement the key issues of the paper.

Introduction

Molecular sensors communicating via changes in optical signals have attracted considerable attention during the past decades,[1] basically fueled by rapid developments in instrumentation[2] and advances in contemporary synthetic (receptor) chemistry.[3] Besides metal cations which have been targeted for almost 30 years,[1a,4] inorganic anions and charged as well as neutral organic molecules have especially been focusing research activities in this field since the late 1980s.[3,5] Although several new methodologies, such as differential sensing with sensor arrays,[6] displacement protocols[7] or sensory polymers[8] have been

[†] Universidad Politécnica de Valencia.
[‡] Bundesanstalt für Materialforschung und -prüfung.
[§] Universitat de València.
[||] Present address: Institut für Chemie, Humboldt Universität zu Berlin, Brook-Taylor-Str. 2, D−12489 Berlin, Germany.

(1) (a) de Silva, A. P.; Gunaratne, H. Q. N.; Gunnlaugsson, T.; Huxley, A. J. M.; McCoy, C. P.; Rademacher, J. T.; Rice, T. E. *Chem. Rev.* **1997**, *97*, 1515−1566. (b) *Fluorescent and Luminescent Probes for Biological Activity*; Mason, W. T., Ed.; Academic: San Diego, 1999; 2nd Edn. (c) Special Issue on "Luminescent Sensors", *Coord. Chem. Rev.* **2000**, *205*. (d) *Optical Sensors and Switches*; Ramamurthy, V., Schanze, K. S., Eds.; Marcel Dekker: New York, 2001. (e) Bernhardt, P. V.; Moore, E. G. *Aust. J. Chem.* **2003**, *56*, 239−258.

(2) See for instance (a) the biennial reviews on "Molecular Fluorescence, Phosphorescence, and Chemiluminescence Spectrometry" (e.g. Agbaria, R. A.; Oldham, P. B.; McCarroll, M.; McGown, L. B.; Warner, I. M. *Anal. Chem.* **2002**, *74*, 3952−3962.) and (b) "Fiber-Optic Chemical Sensors and Biosensors" (e.g., Wolfbeis, O. S. *Anal. Chem.* **2002**, *74*, 2663−2678.) in *Anal. Chem.* or the "Springer Series on Fluorescence, Methods and Applications", (c) *New Trends in Fluorescence Spectroscopy*; Valeur, B., Brochon, J.-C., Eds.; Springer: Berlin, 2001. (d) *Fluorescence Spectroscopy, Imaging and Probes*; Kraayenhof, R., Visser, A. J. W. G., Gerritsen, H. C., Eds.; Springer: Berlin, 2002.

(3) See for instance the illustrative collections of reviews in the Special Issues on "Molecular Recognition", *Chem. Rev.* **1997**, *97*, 1231−1734, "Model Systems", *Curr. Opin. Chem. Biol.* **1997**, *1*, 439−620, or "35 Years of Synthetic Anion Receptor Chemistry 1968−2003", *Coord. Chem. Rev.* **2003**, *240*.

(4) Löhr, H.-G.; Vögtle, F. *Acc. Chem. Res.* **1985**, *18*, 65−72. Tsien, R. Y. *Methods Cell Biol.* **1989**, *30*, 127−156. Rurack, K. *Spectrochim. Acta, Part A* **2001**, *57*, 2161−2195. de Silva, A. P.; McCaughan, B.; McKinney, B. O. F.; Querol, M. *Dalton Trans.* **2003**, 1902−1913.

(5) Snowden, T. S.; Anslyn, E. V. *Curr. Opin. Chem. Biol.* **1999**, *3*, 740−746. Various contributions to Special Issue on "Chemical Sensors", *Chem. Rev.* **2000**, *100*, 2477−2738. Beer, P. D.; Gale, P. A. *Angew. Chem., Int. Ed.* **2001**, *40*, 486-516. Martínez-Máñez, R.; Sancenón, F. *Chem. Rev.* **2003**, *103*, 4419−4476. Fabbrizzi, L.; Licchelli, M.; Taglietti, A. *Dalton Trans.* **2003**, 3471−3479.

(6) (a) Lavigne, J. J.; Anslyn, E. V. *Angew. Chem., Int. Ed.* **2001**, *40*, 3118−3130. (b) Wiskur, S. L.; Floriano, P. N.; Anslyn, E. V.; McDevitt, J. T. *Angew. Chem., Int. Ed.* **2003**, *42*, 2070−2072. (c) García-Acosta, B.; Albiach-Martí, X.; García, E.; Gil, L.; Martínez-Máñez, R.; Rurack, K.; Sancenón, F.; Soto, J. *Chem. Commun.* **2004**, 774−775.

(7) Metzger, A.; Anslyn, E. V. *Angew. Chem., Int. Ed.* **1998**, *37*, 649−652. Fabbrizzi, L.; Leone, A.; Taglietti, A. *Angew. Chem., Int. Ed.* **2001**, *40*, 3066−3069. Prohens, R.; Martorell, G.; Ballester, P.; Costa, A. *Chem. Commun.* **2001**, 1456−1457. Han, M. S.; Kim, D. H. *Angew. Chem., Int. Ed.* **2002**, *41*, 3809−3811. Takahashi, Y.; Pacheco Tanaka, D. A.; Matsunaga, H.; Suzuki, T. M. *J. Chem. Soc., Perkin Trans. 2* **2002**, 759−762.

 10.1021/ja045683n CCC: $30.25

developed for particular problems connected to the recognition and signaling of chemical species, approaches utilizing distinct (bio)molecules still play the leading role. This is especially the case when the application lies in the field of in situ sensing and for rapid screening applications. Although a plethora of sensor molecules has been created so far, rational design strategies for chemosensors,[9] biosensors,[10] or sensor materials[11] are still in a minority. On the other hand, such rational concepts are indispensable for the development of sensing systems for more challenging analytes such as for instance certain individual members or subgroups of chemical compound families. In such a case, when the aim is, e.g., the detection of a certain amino acid, C-5 sugars or long-chain carboxylic acids in a biological medium that usually contains a (larger) variety of closely related derivatives, the sensing device has to be more sophisticated than simply to be able to recognize a certain functional group. At the same time, not only selectivity should fit the purpose, but the processes that generate the information and transduce it to the user have to be powerful and unequivocal to fulfill analytical needs with respect to sensitivity and instrumentation. To avoid that time-consuming synthesis, testing, and serendipity govern the development of such a device, the construction of an optical sensor for challenging targets should make full use of rational strategies available in the fields of organic and/or inorganic supramolecular chemistry, photochemistry and photophysics.

Being engaged with the development of chemical sensing systems for anions for several years,[6c,12] we became aware of the disproportion that exists between the importance of a certain type of organic carboxylates and the lack of sensors for these target compounds. Following the literature, it is apparent that sensor molecules for short-chain (mono- or di-) carboxylates and benzoates are abundant.[6c,12,13] However, to the best of our knowledge, no sensors have yet been reported for long-chain carboxylates, the anions of fatty acids. This is astonishing as free fatty acids (FFAs), whether in neutral or anionic form, are ubiquitous chemical compounds and play an outstanding role in many different areas that concern life at various levels. For instance, the presence of FFAs in water allows to derive information on water quality and influences the rain-forming process in the atmosphere due to the compounds' surface-active properties.[14] The sensory and dietetic quality of food often depends on the amount of naturally occurring FFAs or FFAs that are produced during storage, technological processing or cooking of foodstuff.[15] FFAs can also determine the quality and performance of industrial products such as, e.g., hydraulic oils or (bio)diesels.[16] In biochemistry, long-chain carboxylic acids and carboxylates are some of the most prominent metabolic effectors and indicators. For example, the increase in plasma FFA concentration in livestock under long-distance transport or (pre-)slaughter conditions is an indicator of stress.[17] Although the mechanisms involved in the membrane transport of long-chain carboxylates are still a matter of controversy,[18] their role in various metabolic disorders and diabetic diseases such as type 2 diabetes or certain cardiovascular diseases is well-established today.[19]

Concerning the requirements on a sensor for fatty carboxylates, the sum parameter of FFA anion concentration is often a reliable measure and reveals sufficient information on the analytical problem in many cases. However, especially for particular clinical problems related to the dietary use of medium-chain fatty acids (basically C-8 and C-10), a discrimination between carboxylates of less and more then 10 carbon atoms in the chain would be desirable. Medium-chain triacylglycerols were proposed as weight-lowering agents, ergogenic aids for optimal performance of athletes, and were claimed to help reduce the risk of cardiovascular diseases and serve as an important tool in treating various diseases connected to malfunctions of lipid metabolism.[20] In all of these cases, the special diets rely on a substitution of long-chain for medium-chain fats

(8) McQuade, D. T.; Pullen, A. E.; Swager, T. M. *Chem. Rev.* **2000**, *100*, 2537−2574. Ho, H. A.; Leclerc, M. *J. Am. Chem. Soc.* **2003**, *125*, 4412−4413. Kim, T.-H.; Swager, T. M. *Angew. Chem., Int. Ed.* **2003**, *42*, 4803−4806. Aldakov, D.; Anzenbacher, Jr, P. *J. Am. Chem. Soc.* **2004**, *126*, 4752−4753. Kwak, G.; Fujiki, M.; Masuda, T. *Macromolecules* **2004**, *37*, 2422−2426.

(9) Chin, J.; Walsdorff, C.; Stranix, B.; Oh, J.; Chung, H.-J.; Park, S.-M.; Kim, K. *Angew. Chem., Int. Ed.* **1999**, *38*, 2756−2759. Schneider, S. E.; O′Neil, S. N.; Anslyn, E. V. *J. Am. Chem. Soc.* **2000**, *122*, 542−543. Tanaka, K.; Miura, T.; Umezawa, N.; Urano, Y.; Kikuchi, K.; Higuchi, T.; Nagano, T. *J. Am. Chem. Soc.* **2001**, *123*, 2530−2536.

(10) Marvin, J. S.; Hellinga, H. W. *Proc. Natl. Acad. Sci. U.S.A.* **2001**, *98*, 4955−4960. Miyawaki, A.; Nagai, T.; Mizuno, H. *Curr. Opin. Chem. Biol.* **2003**, *7*, 557−562. Hutschenreiter, S.; Neumann, L.; Radler, U.; Schmitt, L.; Tampe, R. *ChemBioChem* **2003**, *4*, 1340−1344. Ferguson, A.; Boomer, R. M.; Kurz, M.; Keene, S. C.; Diener, J. L.; Keefe, A. D.; Wilson, C.; Cload, S. T. *Nucl. Acids Res.* **2004**, *32*, 1756−1766.

(11) Swager, T. M.; Marsella, M. J.; Zhou, Q.; Newland, R. J. *Mater. Res. Soc. Symp. Proc.* **1996**, *413*, 407−411. Kneas, K. A.; Demas J. N.; DeGraff, B. A.; Periasamy, A. *Microsc. Microanal.* **2000**, *6*, 551−561. Subrahmanyam, S.; Piletsky, S. A.; Piletska, E. V.; Chen, B. N.; Karim, K.; Turner, A. P. F. *Biosens. Bioelectron.* **2001**, *16*, 631−637.

(12) (a) Sancenón, F.; Descalzo, A. B.; Martínez-Máñez, R.; Miranda, M. A.; Soto, J. *Angew. Chem., Int. Ed.* **2001**, *40*, 2640−2643. (b) Sancenón, F.; Martínez-Máñez, R.; Soto, J. *Angew. Chem., Int. Ed.* **2002**, *41*, 1416−1419. (c) Sancenón, F.; Martínez-Máñez, R.; Miranda, M. A.; Segui, M. J.; Soto, J. *Angew. Chem., Int. Ed.* **2003**, *42*, 647−650. (d) Jiménez, D.; Martínez-Máñez, R.; Sancenón, F.; Ros-Lis, J. V.; Benito, A.; Soto, J. *J. Am. Chem. Soc.* **2003**, *125*, 9000−9001. (e) Kovalchuk, A.; Bricks, J. L.; Reck, G.; Rurack, K.; Schulz, B.; Szumna, A.; Weisshoff, H. *Chem. Commun.* **2004**, 1946−1947.

(13) (a) Teulade-Fichou, M.-P.; Vigneron, J.-P.; Lehn, J.-M. *J. Chem. Soc., Perkin Trans. 2* **1996**, 2169−2175. (b) Beer, P. D.; Szemes, F.; Balzani, V.; Salà, C. M.; Drew, M. G. B.; Dent, S. W.; Maestri, M. *J. Am. Chem. Soc.* **1997**, *119*, 11864−11875. (c) Takeuchi, M.; Imada, T.; Shinkai, S. *Angew. Chem., Int. Ed.* **1998**, *37*, 2096−2099. (d) Beer, P. D.; Timoshenko, V.; Maestri, M.; Passaniti, P.; Balzani, V. *Chem. Commun.* **1999**, 1755−1756. (e) Fabbrizzi, L.; Licchelli, M.; Parodi, L.; Poggi, A.; Taglietti, A. *Eur. J. Inorg. Chem.* **1999**, 35−39. (f) Watanabe, S.; Higashi, N.; Kobayashi, M.; Hamanaka, K.; Takata, Y.; Yoshida, K. *Tetrahedron Lett.* **2000**, *41*, 4583−4586. (g) Yoshida, H.; Saigo, K.; Hiratani, K. *Chem. Lett.* **2000**, 116−117. (h) Mei, M.; Wu, S. *New J. Chem.* **2001**, *25*, 471−475. (i) Lee, D. H.; Lee, K. H.; Hong, J.-I. *Org. Lett.* **2001**, *3*, 5−8. (j) Montalti, M.; Prodi, L.; Zaccheroni, N.; Charbonnière, L.; Douce, L.; Ziessel, R. *J. Am. Chem. Soc.* **2001**, *123*, 12694−12695. (k) Kato, R.; Nishizawa, S.; Hayashita, T.; Teramae, N. *Tetrahedron Lett.* **2001**, *42*, 5053−5056. (l) Gunnlaugsson, T.; Harte, A. J.; Leonard, J. P.; Nieuwenhuyzen, M. *Chem. Commun.* **2002**, 2134−2135. (m) Gunnlaugsson, T.; Davis, A. P.; O'Brien, J. E.; Glynn, M. *Org. Lett.* **2002**, *4*, 2449−2452. (n) Raker, J.; Glass, T. E. *J. Org. Chem.* **2002**, *67*, 6113−6116. (o) Kubo, Y.; Ishihara, S.; Tsukahara, M.; Tokita, S. *J. Chem. Soc., Perkin Trans. 2* **2002**, 1455−1460. (p) Zhang, X.; Guo, L.; Wu, F.-Y.; Jiang, Y.-B. *Org. Lett.* **2003**, *5*, 2667−2670. (q) Gunnlaugsson, T.; Kruger, P. E.; Lee, T. C.; Parkesh, R.; Pfeffer, F. M.; Hussey, G. M. *Tetrahedron Lett.* **2003**, *44*, 6575−6578.

(14) Saliot, A.; Bouloubassi, I.; Lorreboireau, A.; Trichet, J.; Poupet, P.; Charpy, L. *Coral Reefs* **1994**, *13*, 243−247. Seidl, W. *Atmos. Environ.* **2000**, *34*, 4917−4932. Pedersen, J. A.; Yeager, M. A.; Suffet, I. H. *Water Sci. Technol.* **2002**, *45*, 103−110.

(15) Ferrer, E.; Alegria, A.; Farre, R.; Abellan, P.; Romero, F. *Food Sci. Technol. Int.* **1999**, *5*, 447−461. Gertz, C. *Eur. J. Lipid Sci. Technol.* **2000**, *102*, 566−572. Tan, C. P.; Man, Y. B. C.; Jinap, S.; Yusoff, M. S. A. *J. Am. Oil Chem. Soc.* **2001**, *78*, 1227−1232.

(16) Vosmann, K.; Sander, B.; Spilker, M.; Ihrig, H. *Fett Wiss. Technol.* **1995**, *97*, 287−288. Canakci, M.; Van Gerpen, J. *Trans. ASAE* **1999**, *42*, 1203−1210.

(17) Shaw, F. D.; Tume, R. K. *Meat Sci.* **1992**, *32*, 311−329. Knowles, T. G.; Warriss, P. D.; Brown, S. N.; Kestin, S. C. *Vet. Rec.* **1994**, *134*, 107−110. Ruane, N. M.; Komen, H. *Aquaculture* **2003**, *218*, 685−693.

(18) (a) Kamp, F.; Hamilton, J. A. *Biochemistry* **1993**, *32*, 11074−11086. (b) Schmider, W.; Fahr, A.; Voges, R.; Gerok, W.; Kurz, G. *J. Lipid Res.* **1996**, *37*, 739−753. (c) Stahl, A. *Pflügers Arch.* **2004**, *447* 722−727.

(19) (a) Roden, M.; Price, T. B.; Perseghin, G.; Falk Petersen, K.; Rothman, D. L.; Cline, G. W.; Shulman, G. I. *J. Clin. Invest.* **1996**, *97*, 2859−2865. (b) Saleh, J.; Sniderman, A. D.; Cianflone, K. *Clin. Chim. Acta* **1999**, *286*, 163−180. (b) Carvajal, K.; Moreno-Sánchez, R. *Arch. Med. Res.* **2003**, *34*, 89−99.

and fatty acids,[21] which does not only entail an adaption of the respective methods for product control, but also raises new toxicological and analytical questions,[22] in the latter case especially the discrimination between short- and medium-chain on one hand and long-chain fatty acids on the other hand. Stimulated by these facts and features, we describe in the present contribution the rational design of a chemosensor for the chromogenic and fluorogenic detection of the biochemically important target group of long-chain carboxylates.

Design Considerations

Choice of the Primary Recognition and Signaling Unit. Our aim was to develop a sensor platform that can be operated with one of the most convenient reporter media in chemical sensing, i.e., light. Besides spectrophotometry, especially fluorometric techniques are generally characterized by a high degree of specificity (via choice of excitation and emission wavelengths) and enable the user to access a wealth of information (e.g., spectral and intensity changes, fluorescence lifetime) in rather straightforward and fast measurement protocols. Many high-throughput screening, microscopy or other microplate-based instrumentation uses (laser) excitation and fluorescence detection for data acquisition,[23] and communicating with light is at the heart of analytical methods employing fiber optics.[2b] Most frequently, argon ion and frequency-doubled Nd:YAG lasers or laser diodes are used as light sources here, being conventionally operated at $\lambda \geq 480$ nm. A suitable chromophoric unit should thus absorb in the 450−550 nm region. This requirement excludes the majority of fluorophores used so far in carboxylate sensing, i.e., polycyclic aromatic hydrocarbons (PAH) such as naphthalene, anthracene or pyrene[24] as well as lanthanide ion lumophores that are commonly excited via UV-absorbing organic antennas.[13j,k,m,25] Additionally, most coumarins, polyphenyls or oxazoles and related compounds are inadequate. The dye classes that potentially meet this condition and were thus further taken into consideration by us are styryl, pyrromethene and fluorescein dyes as well as rhodamine and phenoxazinone derivatives.[26] From the point of view of an efficient transduction of the binding event, the second major prerequisite for a signaling unit is that the presence of a guest is indicated by an increase in emission rather than fluorescence quenching, which is adventageous in terms of detection limit, signal-to-noise ratio and fluorescence lifetimes that are specific for a certain complex or host−guest supramolecular ensemble. Thus, another key task concerns the choice of an appropriate photophysical signaling mechanism. Binding of carboxylates can usually be achieved by hydrogen bonding or electrostatic interaction.[27] Most systems that utilize pure electrostatic interaction in the form of coordinative binding to metal ion centers however cancel out due to spectroscopic limitations. Such probes are for instance Zn^{2+} or Cu^{2+} polyamine-anthracene (or other PAH) conjugates or lanthanide ion-based probes that can be usually only excited in the UV. Furthermore, these systems seldomly show guest-amplified luminescence. Better suitable for a facile integration to one of the visible-range chromophores listed above are organic neutral (e.g., amido, urea, thiourea) or charged (e.g., guanidinium, isothiouronium) hydrogen bond donor groups. In principle, signaling can here be accomplished via PET type fluorescence quenching or revival,[28] or through the modulation of an intramolecular charge transfer process. In terms of the generation of strong analyte-induced spectroscopic changes however, hydrogen bond formation is a rather weak force and the respective receptor groups are often considerably weak electron donors or acceptors. Today, the majority of the acetate-responsive sensor molecules operate via PET processes and entail all the applicationary disadvantages addressed before.[24] Significant carboxylate-induced spectral changes are seldomly reported and only in a few special cases, large acetate-induced shifts of absorption and/or fluorescence bands have been reported, e.g., for ternary metal ion-dye-acetate conjugates or certain excimer-forming as well as charge transfer-based dual emissive dyes.[6c,29]

Remaining with these chromophore and hydrogen-bonding receptor classes mentioned in the last paragraph and on the background of the electronic effects that are to be expected upon carboxylate binding, various ways are possible to approximate a suitable sensor molecule: combinatorial techniques, computer-aided design or the utilization of structure−property relationships. Recently, especially combinatorial techniques have attracted much attention and have been employed to generate larger populations of dyes and labels with the aim to accelerate the discovery of fluorophores with specific properties.[30] How-

(20) Bach, A. C.; Ingenbleek, Y.; Frey, A. *J. Lipid Res.* **1996**, *37*, 708−726. Kern, M.; Lagomarcino, N. D.; Misell, L. M.; Schuster, V. *J. Nutr. Biochem.* **2000**, *11*, 288−292. Wächtershäuser, A.; Stein, J. *Ernährungs-Umschau* **2004**, *51*, 144−148.

(21) Varlemann, H. In *Praxishandbuch klinische Ernährung und Infusionstherapie*; Stein, J., Jauch, K. W., Eds.; Springer, Berlin, 2003, pp 677−693.

(22) Mingrone, G.; Greco, A. V.; Capristo, E.; Benedetti G.; Castagneto, M.; Gasbarrini, G. *Clin. Chim. Acta* **1995**, *240*, 195−207. Schmall, T. L.; Brewer, M. S. *J. Food Quality* **1996**, *19*, 295−302. Traul, K. A.; Driedger, A.; Ingle, D. L.; Nakhasi, D. *Food Chem. Toxicol.* **2000**, *38*, 79−98.

(23) Comprehensive and up to date information on the most common and commercially available fluorescent stains and labels in combination with the respective instrumentation is given on the CD-ROM series *The Purdue Cytometry CD-ROM*; Robinson, J. P., Purdue University Cytometry Laboratories: West Lafayette, 1996−2003; Vol. 1−7 and *Purdue Microscopy, Image Analysis and 3D Reconstruction CD-ROM series*; Pawley, J. B., Robinson, J. P., Eds.; Purdue University: West Lafayette, 1998; Vol. 1 or on the web site of the PUCL at http://www.cyto.purdue.edu.

(24) Easily reducible PAH fluorophores are employed in most photoinduced electron transfer (PET) type probes for anions, many of them showing fluorescence quenching upon binding to the electron rich analytes; see e.g. (a) Nishizawa, S.; Kaneda, H.; Uchida, T.; Teramae, N. *J. Chem. Soc., Perkin Trans. 2* **1998**, 2325−2327. (b) Kubo, Y.; Tsukahara, M.; Ishihara, S.; Tokita, S. *Chem. Commun.* **2000**, 653−654. (c) Gunnlaugsson, T.; Davis, A. P.; Glynn, M. *Chem. Commun.* **2001**, 2556−2557. (d) Sasaki, S.; Citterio, D.; Ozawa, S.; Suzuki, K. *J. Chem. Soc., Perkin Trans. 2* **2001**, 2309−2313. (e) Nishizawa, S.; Cui, Y.-Y.; Minagawa, M.; Morita, K.; Kato, Y.; Taniguchi, S.; Kato, R.; Teramae, N. *J. Chem. Soc., Perkin Trans. 2* **2002**, 866−870.

(25) Other examples of lanthanide-based probes that are excited at wavelength below 480 nm are e.g., Bruce, J. I.; Dickins, R. S.; Govenlock, L. J.; Gunnlaugsson, T.; Lopinski, S.; Lowe, M. P.; Parker, D.; Peacock, R. D.; Perry, J. J. B.; Aime, S.; Botta, M. *J. Am. Chem. Soc.* **2000**, *122*, 9674−9684. Yamada, T.; Shinoda, S.; Tsukube, H. *Chem. Commun.* **2002**, 1218−1219. Furthermore, transition metal-complex lumophores with Re^{I} or Ir^{III} centers also absorb in the UV, see e.g., Goodall, W.; Williams, J. A. G. *J. Chem. Soc., Dalton Trans.* **2000**, 2893−2895. Sun, S. S.; Lees, A. J.; Zavalij, P. Y. *Inorg. Chem.* **2003**, *42*, 3445−3453.

(26) In principle, lumophores with Ru^{II} transition metal ion centers also meet the spectral requirements. However, analyte-induced quenching is observed in many cases and due to the inherent nature of the photophysical process that leads to luminescence in these molecules, pronounced complexation-induced spectral shifts that are important for chromogenic or ratiometric fluorescence detection are not to be expected.[13b,d,f]

(27) Fitzmaurice, R. J.; Kyne, G. M.; Douhert, D.; Kilburn, J. D. *J. Chem. Soc., Perkin Trans. 1* **2002**, 841−864. Sensor molecules that were designed for short-chain dicarboxylates, basically α,ω-dicarboxylates, usually have additional signaling modes available, based on geometrical changes upon complexation of the guest, see e.g., refs 13c,f,h,m,n.

(28) PET processes can occur as pure redox processes or can involve the co-transfer of a proton, exemplifying the special case of proton-coupled electron transfer (PCET), see Cukier, R. I.; Nocera, D. G. *Annu. Rev. Phys. Chem.* **1998**, *49*, 337−369. Lebeau, E. L.; Binstead, R. A.; Meyer, T. J. *J. Am. Chem. Soc.* **2001**, *123*, 10535−10544.

(29) Nishizawa, S.; Teramae, N. *Anal. Sci.* **1997**, *13*, 485−488 Suppl. Wu, F.-Y.; Ma, L.-H.; Jiang, Y.-B. *Anal. Sci.* **2001**, *17*, i801-i803. Wu, F.-Y.; Li, Z.; Wen, Z.-C.; Zhou, N.; Zhao, Y.-F.; Jiang, Y.-B. *Org. Lett.* **2002**, *4*, 3203−3205.

Chart 1. Chemical Structures of Selected Amido- or Thiourea-functionalized Fluorescent Dyes as Discussed in the Text. Representative Spectral Data in Alcoholic or (mixed) Aqueous Solution Are: **SITS**, λ_{abs} = 360 nm, λ_{em} = 420 nm;[37a] **ANS** with R = $(CH_3)_2CH-$, λ_{abs} = 377 nm, λ_{em} = Not Reported;[37c] **DMABTUS**, λ_{abs} = 390 nm, λ_{em} = 450 nm;[36a] **SP**, λ_{abs} = 324 nm, λ_{em} = Not Reported;[33e] **AP**, λ_{abs} = 470 nm, λ_{em} = Not Reported.[43a] Bottom Right: Numbering of the Phenoxazinone Skeleton

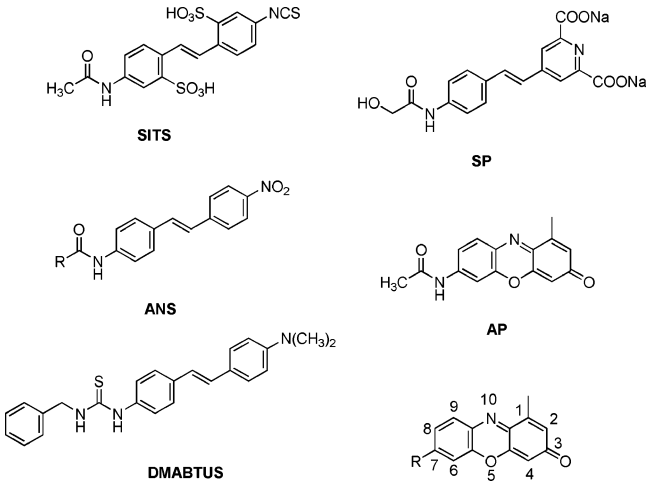

ever, whereas this strategy might be useful in optimizing rather simple dye architectures, the synthetic effort to prepare a library of discrete sensor molecules is extensive and time-consuming. On the other hand, computer-aided screening of virtual libraries might be a valuable tool in receptor design,[31] yet it is currently not applicable to fluorophore development. The theoretical prediction of optical properties, especially in fluorescence, is difficult and still today, computational methods for a comprehensive mapping of excited-state features of larger molecules or even host−guest complexes are very limited. Instead, we relied on structure−property relationships.[32]

Because anionic species are targeted, all the electron-deficient and highly emissive fluorophores such as fluoresceins, pyrromethenes, rhodamines, where the common indication reaction is similar to the PAH-containing PET probes, i.e., signaling would most probably involve an electron transfer from an electron-rich receptor-anion complex to the chromophore, promised to be less suitable and were not considered in the structure−property correlations any further. Furthermore, when scrutinizing the literature on styryl dyes, the lack of long-wavelength absorbing derivatives with simple amido, urea or guanidinium groups is apparent (Chart 1).[33] This fact is most probably due to the complex photophysics that are already exhibited by simple benzanilindes.[34] Additionally, weakly donor-substituted stilbenes that constitute the UV-absorbing and emitting twins of styryl dyes usually show pronounced trans-cis isomerization in the ground and/or excited state due to (multiple) flexible bonds in the chromophore, further complicating the issue.[35] Thus, although various attempts have been made to introduce amido-, urea-, or thiourea-substituted stilbenes as blue fluorescent dyes to biomedical imaging or materials chemistry,[36] only very few derivatives such as **SITS** (4-acetoamido-4′-isothiocyanostilbene-2,2′-disulfonic acid) or 4-alkylamido-4′-nitrostilbenes **ANS** have still some relevance today.[37] As the case is different for the all-rigid phenoxazinone chromophore, a suitable sensor molecule was distilled from a pool of structures by analyzing a "library" of experimental data of various phenoxazinone derivatives that mimic best the potential probe and their respective LFER parameters. So far, 7-dialkylamino derivatives of phenoxazin-3-one[38] and especially benzo[*a*]phenoxazin-5-one (or Nile Red) have been frequently employed as polarity probes in solvent mixtures and confined media,[39] for the microenvironment or as FRET partners in biomolecules, and for vapor sensing.[40] However, to the best of our knowledge no phenoxazinone-type fluorescent molecular sensors relying on host−guest recognition and signaling have yet been reported, with the exception of our recent mercury sensor.[41] Additionally, 7-substituted phenoxazin-3-ones fulfill other key requirements on optical sensors such as high photostability and water solubility. Although databases of LFER parameters are often considerably large,[42] this approach implied a restriction to simpler receptor mimics for which tabulated data are available. On the basis of the Hammett constant data tabulated in ref 42, experimental data reported on several 7-*R*-phenoxazin-3-one derivatives by Stužka et al. and Musso and Matthies as well as own experimental data obtained during recent studies,[41,43] we correlated the absorption maxima (Figure 1) as well as fluorescence quantum yields in several solvents with σ_p data. The 7-substituents used for the plots were H, OH,

(30) Loren, J. C.; Siegel, J. S. *Angew. Chem., Int. Ed.* **2001**, *40*, 754−757. Schiedel, M.-S.; Briehn, C. A.; Bäuerle, P. *Angew. Chem., Int. Ed.* **2001**, *40*, 4677−4680. Lee, J. W.; Jung, M.; Rosania, G. R.; Chang, Y. T. *Chem. Commun.* **2003**, 1852−1853.

(31) Lehn, J.-M. *Chem. Eur. J.* **1999**, *8*, 2455−2463. Kubinyi, H. *J. Recept. Signal Transduction Res.* **1999**, *19*, 15−39. Linton, B.; Hamilton, A. D. *Curr. Opin. Chem. Biol.* **1999**, *3*, 307−312.

(32) See e.g., Katritzky, A. R.; Topsom, R. D. In *Advances in Linear Free Energy Relationships*; Chapman, N. B., Shorter, J., Eds.; Plenum: London, 1972; pp 119−141 for a correlation of LFER and absorption data.

(33) (a) Mishra, A.; Behera, R. K.; Behera, P. K.; Mishra, B. K.; Behera, G. B. *Chem. Rev.* **2000**, *100*, 1973−2012. (b) Papper, V.; Likhtenshtein, G. I. *J. Photochem. Photobiol., A Chem.* **2001**, *140*, 39−52. (c) Grabowski, Z. R.; Rotkiewicz, K.; Rettig, W. *Chem. Rev.* **2003**, *103*, 3899−4031. Moreover, simple derivatives such as styrylpyridines still absorb and emit in the same UV-wavelength range as stilbenes, e.g., (d) Doty, J. C.; Williams, J. L. R.; Grisdale, P. J. *Can. J. Chem.* **1969**, *47*, 2355−2359. (e) Lamture, J. B.; Iverson, B.; Hogan, M. E. *Tetrahedron Lett.* **1996**, *37*, 6483−6486.

(34) Braun, D.; Rettig, W.; Delmond, S.; Létard, J.-F.; Lapouyade, R. *J. Phys. Chem. A* **1997**, *101*, 6836−6841. Lewis, F. D.; Long, T. M. *J. Phys. Chem. A* **1998**, *102*, 5327−5332. Zhang, X.; Wang, C.-J.; Liu, L.-H.; Jiang, Y.-B. *J. Phys. Chem. B* **2002**, *106*, 12432−12440.

(35) Waldeck, D. H. *Chem. Rev.* **1991**, *91*, 415−436. Saltiel, J.; Charlton, J. L. In *Rearrangements in Ground and Excited States*; de Mayo, P., Ed.; Academic: New York, Vol. 3., 1980; pp. 25−89. Seydack, M.; Bendig, J. *J. Phys. Chem. A* **2001**, *105*, 5731−5733. Han, W.-G.; Lovell, T.; Liu, T.; Noodleman, L. *ChemPhysChem* **2002**, *3*, 167−178.

(36) (a) Sinsheimer, J. E.; Stewart, J. T.; Burckhalter, J. H. *J. Pharm. Sci.* **1968**, *57*, 1938−1945. (b) Tsibouklis, J.; Mukherjee, S.; Cresswell, J.; Petty, M. C.; Feast, W. J. *J. Mol. Electron.* **1990**, *6*, 221−223. (c) Chen, D.-W.; Beuscher, IV, A. E.; Stevens, R. C.; Wirsching, P.; Lerner, R. A.; Janda, K. D. *J. Org. Chem.* **2001**, *66*, 1725−1732.

(37) (a) Benjamin, M. A.; Katz, I. J. *Stain Technol.* **1970**, *45*, 57−62. (b) Papper, V.; Likhtenshtein, G. I.; Medvedeva, N.; Khoudyakov, D. V. *J. Photochem. Photobiol., A Chem.* **1999**, *122*, 79−85. (c) Mikes, F.; Strop, P.; Kalal, J. *Makromol. Chem.* **1974**, *175*, 2375−2391. (d) Gonzalez-Benito, J.; Mikes, F.; Baselga, J.; Lemetyinemm, H. *J. Appl. Polym. Sci.* **2002**, *86*, 2992−3000.

(38) (a) Brugel, T. A.; Williams, B. W. *J. Fluoresc.* **1993**, *3*, 69−76. (b) Otsuki, S.; Taguchi, T. *J. Photochem. Photobiol., A Chem.* **1997**, *104*, 189−195.

(39) Deye, J. F.; Berger, T. A.; Anderson, A. G. *Anal. Chem.* **1990**, *62*, 615−622. Greenspan, P.; Fowler, S. D. *J. Lipid Res.* **1985**, *26*, 781−789. Moreno, E. M.; Levy, D. *Chem. Mater.* **2000**, *12*, 2334−2340.

(40) Sackett, D. L.; Knutson, J. R.; Wolff, J. *J. Biol. Chem.* **1990**, *25*, 14899−14906. Meinershagen, J. L.; Bein, T. *J. Am. Chem. Soc.* **1999**, *121*, 448−449. Wichmann, O.; Schultz, C. *Chem. Commun.* **2001**, 2500−2501.

(41) Descalzo, A. B.; Martínez-Máñez, R.; Radeglia, R.; Rurack, K.; Soto, J. *J. Am. Chem. Soc.* **2003**, *125*, 3418−3419.

(42) Hansch, C.; Leo, A.; Taft, R. W. *Chem. Rev.* **1991**, *91*, 165−195.

(43) (a) Musso, H.; Matthies, H. G. *Chem. Ber.* **1957**, *90*, 1814−1827. (b) Stužka, V.; Golovina, A. P.; Alimarin, I. P. *Collect. Czech. Chem. Commun.* **1969**, *34*, 221−228. (c) Stužka, V.; Šimánek, V. *Collect. Czech. Chem. Commun.* **1970**, *37*, 1121−1129.

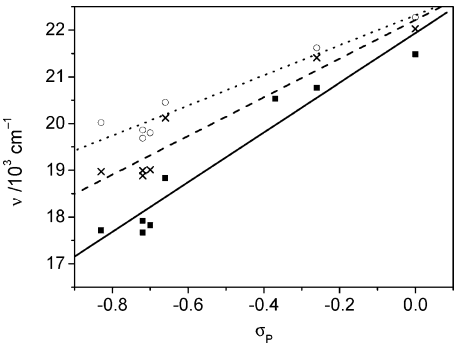

Figure 1. Plots and fits of $\tilde{\nu}_{abs}$(max) vs σ_P in Et_2O (circles, dotted line), MeCN (crosses, dashed line), and MeOH (squares, solid line).

Table 1. Results and Parameters of the Correlations (eq. $y = mx + b$; $\sigma_P = -0.26$ for the urea group)

correlation	m	b	*r*	value for **1v**[a]	value for **1**[b]
$\tilde{\nu}_{abs}^{max}$ (MeOH) vs σ_P	5313	21935	0.964	20533 cm^{-1}	20768 cm^{-1}
$\tilde{\nu}_{abs}^{max}$ (MeCN) vs σ_P	4134	22215	0.959	21140 cm^{-1}	21413 cm^{-1}
$\tilde{\nu}_{abs}^{max}$ (Et_2O) vs σ_P	3217	22318	0.966	21481 cm^{-1}	21621 cm^{-1}
Φ_f(MeOH) vs σ_P	−0.257	0.005	0.988	0.059	0.065

[a] As obtained from the fit. [b] Measured, see Table 2.

Chart 2. Molecular Sensor Dyes and Model Compounds. **1v** Is the Virtual Analogue of **1** and Was Not Synthesized or Studied Experimentally

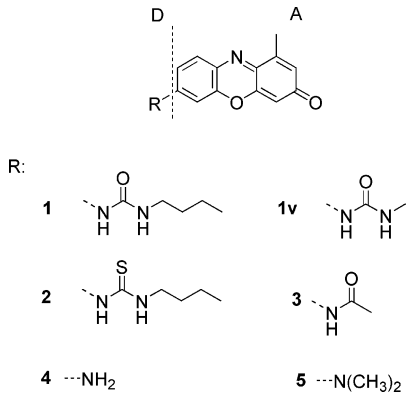

O^-, NH_2, NHCOMe, and various alkylated amino groups. Inspecting the results of the correlations summarized in Table 1, satisfactory correlations were obtained for plots of the absorption maxima in various solvents as well as the fluorescence quantum yield Φ_f in MeOH vs σ_P.[44] Moreover, the negative slope of the Φ_f vs σ_P correlation and the positive slopes of the $\tilde{\nu}_{abs}$ vs σ_P plots or, in other words, the exchange of a less electron-rich donor substituent (exemplifying the free anion receptor site) for a more electron-rich group (exemplifying the receptor-anion complex) suggest that anion binding should lead to analytically advantageous bathochromic shifts and amplified fluorescence. Taking further the facility of synthesis into account, the most promising candidate which crystallized from the virtual pool of structures was the 7-urea derivative **1v** (see structure in Chart 2).

Choice of the Medium that Determines the Selectivity. To obtain the desired selectivity for long-chain carboxylates, the only other "functional" characteristic of the target analytes that can be addressed is their long alkyl chain. As no direct functional receptor group for the binding of long alkyl chains is available, the creation of a molecular sensor in the classical sense would presumably not lead to success, despite the tremendous synthetic effort that would be required to equip a probe molecule such as **1v** with for instance a larger synthetic hydrophobic pocket. Alternatively, it is helpful to consider how nature deals with such problems. The success of many proteins in tightly binding a designated substrate with rather conventional hydrogen bonding receptors in aqueous media lies in the shielding of the active site-substrate complex against competing water molecules. The active regions of proteins are usually embedded in a flexible (super)structure, where entrance of the substrate induces a reorientation of the binding sites (i.e., "induces the fit") and entails a closing of the pocket and the squeezing out of water, thereby enhancing the stability of conventional hydrogen bonded complexes. In effect, the protein "extracts" the substrate from the environment before commencing with the biochemical reaction. Such concerted and autonomous action at the molecular level is currently not achievable with synthetic chemical analogues.[45] However, certain architectures that mimic simple features of biological structures such as membranes or (ion) channels and their specific selection properties or surface activities have recently been constructed by materials chemistry-based tuning of rigid but porous, inorganic or organic host structures with secondary, organic, or mixed organic−inorganic functionalization of the (inner) surface.[46] Since the discovery of periodic mesoporous materials in 1992,[47] various routes of functionalizing their inner surface have been reported, to yield hybrid materials with improved adsorption, extraction, ion exchange, or catalytic abilities.[48] Due to their narrow and controlled pore size distribution in ordered hexagonal channels with comparatively large pore openings[49] as well as their facile synthesis and robustness, especially siliceous MCM-41 materials have increasingly gained popularity here. Inner surface functionalization can be obtained by co-condensation or postsynthetic covalent grafting of organic groups.[50] Moreover, not only monofunctionalization but successive inclusion of different organic moieties is possible, yieliding higher-order hybrid materials that can be seen as a first step toward "biomimetic" or "enzyme mimicking" nanomaterials.[51] From the viewpoint of engineering optical hybrid materials, microscopic mesoporous siliceous hosts

(44) Suitable and reliable Φ_f data are less abundant in the literature, and thus an analysis was only carried out for MeOH data.

(45) Vogel, V. *Mater. Res. Bull.* **2002**, *27*, 972−978.
(46) For entirely organic or metallo-organic functional mesoscopic structures of various topologies, see Scrimin, P.; Tecilla, P. *Curr. Opin. Chem. Biol.* **1999**, *3*, 730−735. Nguyen, S. T.; Gin, D. L.; Hupp, J. T.; Zhang, X. *Proc. Natl. Acad. Sci. U.S.A.* **2001**, *98*, 11849−11850. Gokel, G. W.; Mukhopadhyay, A. *Chem. Soc. Rev.* **2001**, *30*, 274−286. Bong, D. T.; Clark, T. D.; Granja, J. R.; Ghadiri, M. R. *Angew. Chem., Int. Ed.* **2001**, *40*, 988−1011.
(47) Kresge, C. T.; Leonowicz, M. E.; Roth, W. J.; Vartuli, J. C.; Beck, J. S. *Nature* **1992**, *359*, 710−712.
(48) Moller, K.; Bein, T. *Chem. Mater.* **1998**, *10*, 2950−2963.
(49) With respect to intrapore functionalization as well as active intrapore chemistry (catalysis, ion-exchange, molecular recognition, etc.), especially the larger pore openings present the main advantage of mesoporous MCM-41 or MCM-48 materials as compared to zeolites. Furthermore, the well-defined three-dimensional structure and highly organized arrangement of these materials amplify the favorable features of organically modified silicas (ORMOSILs) prepared under mild conditions by sol−gel synthesis (for a review on functional ORMOSILs, see Collinson, M. M. *Crit. Rev. Anal. Chem.* **1999**, *29*, 289−311) and rendered MCM materials most attractive to us.
(50) More sophisticated approaches are currently being developed, see e.g. Zhang, Q.; Ariga, K.; Okabe, A.; Aida, T. *J. Am. Chem. Soc.* **2004**, *126*, 988−989.
(51) Liu, J.; Shin, Y.; Nie, Z.; Chang, J. H.; Wang, L.-Q.; Fryxell, G. E.; Samuels, W. D.; Exarhos, G. J. *J. Phys. Chem. A* **2000**, *104*, 8328−8339. Huh, S.; Wiench, J. W.; Trewyn, B. G.; Song, S.; Pruski, M.; Lin, V. S.-Y. *Chem. Commun.* **2003**, 2364−2365.

possess the advantages of optical transparency in the visible region while guaranteeing fastness toward UV radiation.[52] Accordingly, first attempts to covalently link organic dye molecules to the inner walls of MCM materials have recently been made.[53] In general, the results reported by these researchers were encouraging as the chromophores largely retained their spectroscopic properties when incorporated into the host. This in turn led to the development of a first generation of hybrid sensor materials consisting of mesoporous hosts mono-functionalized with a pH-sensitive fluorescein,[54] a rhodamine that shows diffusion-controlled quenching in the presence of SO_2,[55] or an aminomethylanthracene responding to ATP[56] as well as a chemodosimeter-type sensing material that indicates fluoride[57] by an irreversible chemical reaction involving the host. Furthermore, first examples of bifunctionalized hybrid sensor materials have very recently been described. In one case, fluorophore and receptor units were grafted separately in two steps onto the surface of a siliceous host.[58] The indication of the targeted paramagnetic Cu^{II} ion was then accomplished via fluorescence quenching induced by Cu^{II}-complexed receptor groups in the direct vicinity of fluorophore moieties. Whereas a similar strategy was followed in the design of self-assembled monolayers on glass supports for metal ion or anion sensing systems,[59] Lin et al. introduced systems that operate via chemodosimetrical fluorescence indication by reaction of the target biogenic amines with a chromophore precursor attached to the pore walls.[60,61]

Our strategy to direct the selectivity of a molecular carboxylate sensor toward the target group of primary interest here, long-chain carboxylates, and to install the required discrimination against their short- and medium-chain analogues was thus the following. In a first step, a sensor molecule that is principally suitable to accomplish the signaling reaction is anchored at low concentrations onto the surface of a mesoporous MCM-41 host. Second, the residual active groups of the support material are refunctionalized with a suitable reagent to finally create a particular environment—the "hydrophobic pocket"—inside the pores. This strategy was assumed to lead to a "biomimetic" hybrid sensor material where the desired response is only obtained by an appropriate combination of the single components, the anchored probe molecule and the support's environmental properties.[62] In particular, the UVM-7 material appeared attractive to us for the present purposes. UVM-7 consists of soldered small (12−17 nm) mesoporous particles that generate a bimodal pore system of 3.0−3.2 nm surfactant mesopores and 20−70 nm textural pores.[63] In addition to the high specific surface (∼1200 $m^2\ g^{-1}$), this MCM-41 type material is characterized by a very high accessibility of the pore surface due to its bimodal pore system, guaranteeing fast response times.

Table 2. Spectroscopic Data of **1** in Selected Solvents at 298 K

solvent	λ_{abs} (max)/nm	fwhm$_{abs}$[a] /cm^{-1}	λ_{em} (max)/nm	$\Delta\tilde{\nu}$ (abs-em)[b] /cm^{-1}	Φ_f	τ_f/ns
H_2O	500	5240	595	3330	0.008	0.14
MeOH	481	4690	582	3740	0.065	0.46
ethylene glycol	492	4720	590	3440	0.065	0.46
glycerol	500	4630	592	3260	0.082	0.61
DMSO	482[c]	4080	595	4160	0.024	0.13
MeCN	467	4700	589	4430	0.015	0.09
acetone	468	4370	588	4410	0.010	0.06
Et_2O	461	3950	579	4670	0.001	<0.01

[a] Full width at half-maximum. [b] Calculated after conversion of the spectra to the energy scale, taking into account a further correction procedure for the emission spectra.[65] [c] $\epsilon_{max} = 13\,460 \pm 280$ cm^{-1} M^{-1} from $N = 8$ experiments.

Synthesis, Spectroscopic Properties, and Performance of the Molecular Sensors

To increase the general solubility behavior and the stability of the target probe structure, we set out to synthezise the *N*-butyl urea derivative of **1v**, **1**. For this purpose, a high excess of the corresponding isocyanate was reacted with 7-aminophenoxazinone **4**,[64] the large amount of functional precursor being necessary due to the poor reactivity of the amino group in **4**.

Spectroscopic Properties of 1, 3−5. Selected spectroscopic data of **1** and the model compounds **3**−**5** in various solvents are collected in Tables 2 and 3, and a set of representative absorption and fluorescence spectra of **1**, **3**−**5** in a highly polar, aprotic solvent is presented in Figure 2. Before discussing the trends of the experimental data within this series of compounds with respect to the underlying photophysical mechanisms, it is helpful to compare the spectroscopic properties measured for **1** in solution with those values obtained for **1v** from the structure−property correlations, to get a first idea of the suitability of the selection procedure employed here for the fluorophore platform. For instance, absorption maxima of $\lambda_{abs} = 467$ nm for **1** in MeCN (Figure 2, Table 2) and 473 nm for **1v** calculated from the $\lambda_{abs}-\sigma_P$ correlation (Figure 1, Table 1) as well as fluorescence quantum yields of 0.059 (**1v**) vs 0.065 (**1**) in methanol clearly reveal the excellent applicability of the design approach. Equally good agreements are obtained for the other absorption and fluorescence parameters where a sufficient amount of

(52) Schulz-Ekloff, G.; Wöhrle, D.; van Duffel, B.; Schoonheydt, R. A. *Micropor. Mesopor. Mater.* **2002**, *51*, 91−138.
(53) (a) Fowler, C. E.; Lebeau, B.; Mann, S. *Chem. Commun.* **1998**, 1825−1826. (b) Lebeau, B.; Fowler, C. E.; Hall, S. R.; Mann, S. *J. Mater. Chem.* **1999**, *9*, 2279−2281. (c) Ganschow, M.; Wark, M.; Wöhrle, D.; Schulz-Ekloff, G. *Angew. Chem., Int. Ed.* **2000**, *39*, 160−163.
(54) Wirnsberger, G.; Scott, B. J.; Stucky, G. D. *Chem. Commun.* **2001**, 119−120.
(55) Wark, M.; Rohlfing, Y.; Altindag, Y.; Wellmann, H. *Phys. Chem. Chem. Phys.* **2003**, *5*, 5188−5194.
(56) Descalzo, A. B.; Jiménez, D.; Marcos, M. D.; Martínez-Máñez, R.; Soto, J.; El Haskouri, J.; Guillem, C.; Beltrán, D.; Amorós, P.; Borrachero, M. V. *Adv. Mater.* **2002**, *14*, 966−969.
(57) Descalzo, A. B.; Jiménez, D.; El Haskouri, J.; Beltrán, D.; Amorós, P.; Marcos, M. D.; Martínez-Máñez, R.; Soto, J. *Chem. Commun.* **2002**, 562−563.
(58) Brasola, E.; Mancin, F.; Rampazzo, E.; Tecilla, P.; Tonellato, U. *Chem. Commun.* **2003**, 3026−3027.
(59) Crego-Calama, M.; Reinhoudt, D. N. *Adv. Mater.* **2001**, *13*, 1171−1174. Basabe-Desmonts, L.; Beld, J.; Zimmerman, R. S.; Hernando, J.; Mela, P.; Garcia Parajo, M. F.; van Hulst, N. F.; van den Berg, A.; Reinhoudt, D. N.; Crego-Calama, M. *J. Am. Chem. Soc.* **2004**, *126*, 7293−7299.
(60) Lin, V. S.-Y.; Lai, C.-Y.; Huang, J.; Song, S.-A.; Xu, S. *J. Am. Chem. Soc.* **2001**, *123*, 11510−11511. Radu, D. R.; Lai, C.-Y.; Wiench, J. W.; Pruski, M.; Lin, V. S.-Y. *J. Am. Chem. Soc.* **2004**, *126*, 1640−1641.
(61) It should be noted that this research area is rapidly expanding at present, with first reports on e.g. organic-metalloorganic hybrid sensor materials (Das, G.; Onouchi, H.; Yashima, E.; Sakai, N.; Matile, S. *ChemBioChem* **2002**, *3*, 1089−1096.), hybrid photoactive switches (Yagi, S.; Minami, N.; Fujita, J.; Hyodo, Y.; Nakazumi, H.; Yazawa, T.; Kami, T.; Hyder Ali, A. *Chem. Commun.* **2002**, 2444−2445.) or electrochemical sensing materials based on porous silicas and functionalized with organic groups (Jiménez-Morales, A.; Galván, J. C.; Aranda, P. *Electrochim. Acta* **2002**, *47*, 2281−2287.) having been published lately.
(62) With respect to the choice of a signaling unit it is important to note that dyes with flexible double bonds which are bound to a hydrophobic backbone/microenvironment can show enhanced trans-cis isomerization yields when such hybrids are employed in hydrophilic media.[37c] The use of rigid fluorophores seems thus to be advisable.
(63) El Haskouri, J.; Ortiz de Zárate, D.; Guillem, C.; LaTorre, J.; Caldés, M.; Beltrán, A.; Beltrán, D.; Descalzo, A. B.; Rodríguez-López, G.; Martínez-Máñez, R.; Marcos, M. D.; Amorós, P. *Chem. Commun.* **2002**, 330−331.
(64) Musso, H.; Wager, P. *Chem. Ber.* **1961**, *94*, 2551−2561.

Table 3. Selected Spectroscopic Data of **3**−**5** at 298 K

	solvent	λ_{abs} (max)/nm	fwhm$_{abs}$ cm^{-1}	λ_{em} (max)/nm	$\Delta\tilde{\nu}$ (abs-em)[a]/ cm^{-1}	Φ_f	ref
3	H_2O	476	7820	596	4250	0.007	*b*
	DMSO	467	6520	602	4800	0.004	*b*
	Et_2O	449	7350	576	4950	0.001	*b*
4	H_2O	560	3040	593	1000	0.222	*c*
	DMSO	528	3240	597	2220	0.591	*c*
	Et_2O	488	3700	568	2970	0.043	*c*
5	H_2O	593	2410	630	1150	0.052	*d*
	DMSO	547	3200	626	2290	0.601	*c*
	Et_2O	501	3270	567	2510	0.009	*c*

[a] Calculated after conversion of the spectra to the energy scale, taking into account a further correction procedure for the emission spectra.[65] [b] This work. [c] ref 67. [d] ref 41.

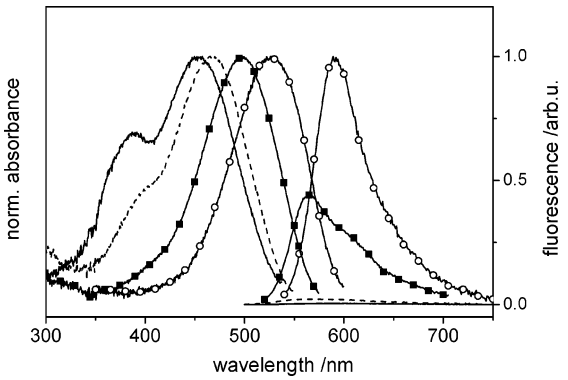

Figure 2. Absorption and emission spectra of **1** (dashed line), **3** (solid line), **4** (squares), and **5** (circles) in MeCN at 298 K.

reliable data was available from the literature. Concerning the solvatochromic and solvatokinetic properties of the phenoxazinones, various trends can be derived from Tables 2 and 3. For all the dyes, the shift in absorption band maximum upon going from apolar to polar aprotic solvents is slightly more pronounced than the corresponding shift of the center of the emission band. This slight reduction in Stokes shifts in, e.g., DMSO as compared to diethyl ether suggests that the differences in dipole moments between the ground and the emissive excited-state species are rather small.[66] At the same time, the fluorescence quantum yields show an opposite trend, i.e., a "negative solvatokinetic behavior" with an increase in fluorescence yield with increasing solvent polarity. This behavior is especially pronounced for **5**, carrying the electron-rich 7-dimethylamino group. Furthermore, the influence of the electron donating properties of the 7-substitutent is directly obvious from Figure 2. As the donor strength increases from amide (**3**) via urea (**1**) to amino (**4**) and dimethylamino (**5**), the spectral bands gradually shift to longer wavelengths and the overall fluorescence emission increases as well. At the same time, the differences between the absorption band positions in DMSO and Et_2O of the four compounds, $\Delta\tilde{\nu}_{abs}(Et_2O-DMSO) = 950\ cm^{-1}$ for **1**, 850 cm^{-1} for **3**, 1530 cm^{-1} for **4** and 1680 cm^{-1} for **5**, correlate well with the theoretically obtained ground-state dipole moments[66] and give further evidence to the electronic influence of the group in the 7-position. Upon changing the environment from aprotic to protic solvents, a reduction in fluorescence quantum yield and Stokes shift are noticed. Concomitantly, a further bathochromic shift of the spectra occurs, and the absorption as well as emission bands show a pronounced reduction in half-width upon increasing the proticity of the solvent.[67] With respect to the underlying photophysical mechanisms, a "negative solvatokinetic behavior" is commonly attributed to the population of a highly emissive charge-transfer excited state.[68] However, whereas such an interpretation is consistent for stilbene or styryl dyes that commonly show negligible shifts in absorption but a strong solvatochromism of their fluorescence, the solvatochromic effects reported here for the phenoxazinones disfavor such an assignment in the present case. Following the literature on phenoxazinones and Nile Red-type dyes, the controversial discussion of the active photophysical mechanisms is apparent. Whereas some researchers invoke specific chromophore-solvent interactions,[38b] others favor the involvement of twisted intramolecular charge transfer (TICT) or other multiple excited states.[69] In many of these studies, the solvent range considered is rather narrow (e.g., restricted to alcohols) and seldomly the works rely on the investigation of mechanistically important model compounds. For instance, our recent studies[67] involving the 7-julolidine derivative suggest that interpretations invoking the TICT model are inadequate as this derivative with a sterically fixed 7-amino nitrogen atom shows the highest fluorescence of all the compounds investigated in highly polar media such as DMSO ($\Phi_f = 0.77$).[67] Unfortunately, most papers also neglect the polymethinic nature of such chromophores which can involve entirely different features well-known from indoaniline photochemistry.[70] The results reported above in combination with the negligible influence of the solvent viscosity on the fluorescence quantum yields and lifetimes of **1** as reflected by Φ_f of 0.065 in MeOH ($\eta_{298K} = 0.544$ mPa s) and ethylene glycol (16.1 mPa s) as well as 0.082 in glycerol (934 mPa s)[71] render the dependence of the population of an emissive state on larger intramolecular motions in the excited state, as would be required for twisted intramolecular charge transfer (TICT) fluorescence, rather unlikey (similar observations were made for **5**, see ref 67).

At this point, it is helpful to consider the trends in the rate constants of radiative and nonradiative deactivation, k_r and k_{nr}.[72] Whereas k_r of **1** is largely constant in all the aprotic solvents ($\sim 1.7 \pm 0.1 \times 10^8\ s^{-1}$), this value decreases substantially upon increasing the proticity of the solvent, yielding e.g., $k_r = 1.4 \approx$

(65) Lakowicz, J. R. *Principles of Fluorescence Spectroscopy*; Plenum: New York, 2nd ed., 1999; pp. 52 ff.
(66) Employing the AM1 method, dipole moments of 6.2 D (**1**), 5.2 D (**3**), 6.7 D (**4**), 7.2 D (**5**) are calculated for the optimized ground-state geometries of the dyes discussed here.
(67) Representative data of the model compounds are included in Table 3. A detailed account on the photophysical mechanisms in 7-substituted phenoxazin-3-ones including a variety of other model compounds such as differently alkylated amines and julolidyl derivatives will be published separately, Descalzo, A. B.; Martínez-Máñez, R.; Radeglia, R.; Rurack, K.; Soto, J.; Weisshoff, H., manuscript in preparation.
(68) Rettig, W. *Top. Curr. Chem.* **1994**, *169*, 253−299. Rettig, W.; Rurack, K.; Sczepan, M. In *New Trends in Fluorescence Spectroscopy: Applications to Chemical and Life Sciences*; Valeur, B., Brochon, J. C., Eds.; Springer: Berlin, 2001; pp 125−155.
(69) Sarkar, N.; Das, K.; Nath, D. N.; Bhattacharyya, K. *Langmuir* **1994**, *10*, 326−329. Datta, A.; Mandal, D.; Pal, S. K.; Bhattacharyya, K. *J. Phys. Chem. B* **1997**, *101*, 10221−10225. Krishna, M. M. G. *J. Phys. Chem. A* **1999**, *103*, 3589−3595.
(70) Schwarzenbach, G.; Mohler, H.; Sorge, J. *Helv. Chim. Acta* **1938**, *21*, 1636−1645. Vittum, P. W.; Brown, G. H. *J. Am. Chem. Soc.* **1946**, *68*, 2235−2239. Adachi, M.; Murata, Y.; Nakamura, S. *J. Am. Chem. Soc.* **1993**, *115*, 4331−4338. Morley, J. O.; Fitton, A. L. *J. Phys. Chem. A* **1999**, *103*, 11442−11450.
(71) Viscosity data taken from *CRC Handbook of Chemistry and Physics*; Lide, D. R., Ed.; CRC Press: Boca Raton, 1993, 73rd ed., pp 6-166−6-170.
(72) k_r and k_{nr} are defined here as $k_r = \Phi_f \times \tau_f^{-1}$ and $k_{nr} = (1-\Phi_f) \times \tau_f^{-1}$.

Chart 3. Quinonimine-zwitterion Equilibrium in Indoaniline Dyes

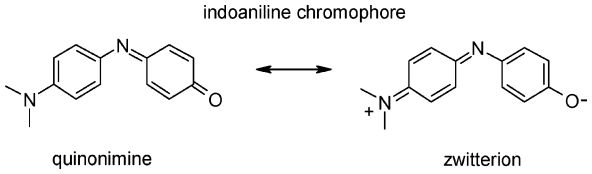

10^8 s^{-1} in methanol and $k_r = 0.6 \approx 10^8$ s^{-1} in water.[73] The latter indicates that the nature of the emissive species changes more strongly as a function of solvent proticity than polarity. On the other hand, starting from highly polar aprotic solvents, k_{nr} decreases signficantly upon going to lower polarity, but is less strongly reduced when moving upward on the proticity scale. The processes leading to fluorescence quenching in these two solvent regimes are thus presumably different. Without further deepening the photophysical discussion here, our forthcoming studies[67] in combination with reports on related merocyanine systems[74] suggest that emission in polar aprotic solvents occurs from a planar excited state that possesses a certain charge transfer character. Especially, the changes observed upon going to alcoholic or aqueous media can then be rationalized as a more pronounced shift of the quinonimine-zwitterion equilibrium (Chart 3) toward the latter, most probably facilitated by increased hydrogen bonding interaction with the solvent. A similar trend i.e., a change in the apparent ionicity (the overall degree in ionic character when both of the forms in Chart 3 are present) or the step from a more polyenic to a more polymethinic nature tentatively accounts for the features found when increasing the donor strength of the 7-substituent. As described above and returning to the key issue of the present paper, the latter leads to an increase in fluorescence yield (Figure 2) and suggests that favorable sensing effects such as anion-enhanced emission can be realized with the present dye platform.[75]

Chromo- and Fluorogenic Anion Signaling Features of 1. Having established the active photophysical mechanisms in the sensor dye, the next step was to test the anion binding features of **1**, in particular with respect to carboxylate indication. Using conditions that are commonly employed for such simple urea-type probes i.e., DMSO as the solvent and the anions as tetraalkylammonium salts,[13] we probed the response of **1** toward various carboxylates as well as a series of monovalent inorganic anions that constitute potential competitors for the recognition site. As would be expected,[13,24,27] acetate modulates the spectroscopic properties of **1**, its presence leading to a deepening of the color from orange to pink as well as a 5-fold enhanced and red-shifted fluorescence (**1**−AcO^-: $\Phi_f = 0.12$, $\tau_f = 0.70$ ns). Both effects indicate that the step from **1** to **1**−AcO^- in Figure 3 is comparable to that from **1** to **4** in Figure 2. In other words, formation of the hydrogen-bonded complex with an anion

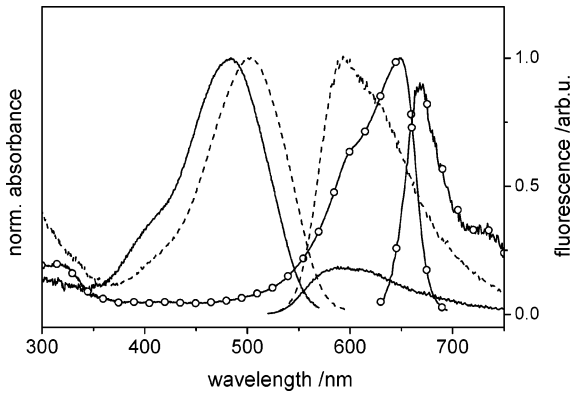

Figure 3. **1** before (solid line) and after the addition of AcO^- (dashed line) and F^- (circles) in DMSO ($c_1 = 4.5 \times 10^{-6}$ M).

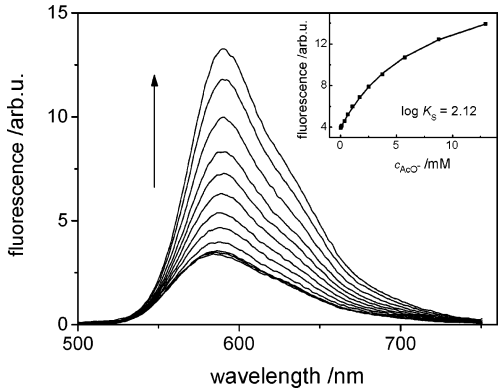

Figure 4. Fluorescence titration spectra for **1** and NBu_4AcO in DMSO ($c_1 = 4.5 \times 10^{-6}$ M, $\lambda_{exc} = 475$ nm). Inset: Plot and fit of the integral fluorescence vs anion concentration, the logK_S of the fit being indicated.

increases the electron density at the nitrogen atom in the 7-position and leads to these analytically advantageous effects. Fluorescence titrations indicate a 1:1 complex stoichiometry with a stability constant log$K_S = 2.12 \pm 0.03$ (Figure 4).

To get an idea of the interference of the carboxylate recognition features by small inorganic anions, the response of **1** toward the latter at a 1500-fold excess of anion vs sensor molecule was taken as a measure. At that excess, $H_2PO_4^-$ induced a 7-fold, Cl^- a 1.4-fold, and HSO_4^- a 1.2-fold enhancement of the fluorescence, all of them with the same characteristics as described before for acetate. NO_3^-, Br^-, as well as I^- had no effect. The response of **1** is thus generally in line with those reported for many other urea-based chromo- and fluorogenic molecular anion sensors.[13,24] Fluoride, on the other hand, induced entirely different changes conceivable with the deprotonation of the dye (Figures 3 and 5). An explanation of the reaction in the presence of F^- is given in conjunction with the results of the NMR experiments further below.

Among the carboxylates tested, a positive response that is qualitatively similar to acetate was only found for benzoate, and a weak response to glucuronate, both of them employed as sodium salts. The medium- and long-chain carboxylates investigated, the analytes of our primary interest, were entirely nonsoluble in DMSO and **1** remained silent toward them. Sodium salicylate as well as trisodium citrate gave also no response.

NMR Spectroscopic Studies of 1 and 3 in the Presence of Anions. The results of the NMR studies with **1** and acetate as well fluoride support the interpretations given in the preceding

(73) Similar trends are found for the model compounds in ref 67.
(74) Dähne, S.; Leupold, D.; Nikolajewski, H.-E.; Radeglia, R. *Z. Naturforsch.* **1965**, *20b*, 1006−1007. Radeglia, R.; Dähne, S. *J. Mol. Struct.* **1970**, *5*, 399−411. Benniston, A. C.; Harriman, A.; McAvoy, C. *J. Chem. Soc., Faraday Trans.* **1998**, *94*, 519−525. Boldrini, B.; Cavalli, E.; Painelli, A.; Terenziani, F. *J. Phys. Chem. A* **2002**, *106*, 6286−6294.
(75) The reduction in emissivity in apolar solvents is most probably connected to enhanced intersystem crossing, which has been reported for related acridines and phenoxazines before (Huber, J. R.; Mantulin, W. W. *J. Am. Chem. Soc.* **1972**, *94*, 3755−3760. Kellmann, A. *J. Phys. Chem.* **1977**, *81*, 1195−1198. Kasama, K.; Kikuchi, K.; Yamamoto, S.; Ujiie, K.; Nishida, Y.; Kokubun, H. *J. Phys. Chem.* **1981**, *85*, 1291−1296.). As this effect is unimportant for the sensor qualities and performance of **1**, the reader is referred to ref 67 for a more detailed description.

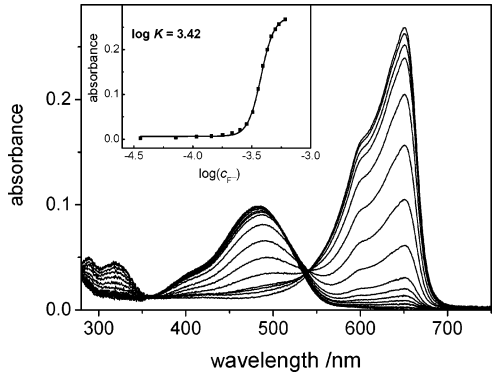

Figure 5. Spectrophotometric titration of **1** with NEt_4F in DMSO ($c_1 = 4.5 \times 10^{-6}$ M). Inset: Plot and fit of $A_{650\ nm}$ vs F^- concentration. For a discussion of the sharpness of the isosbestic point, see caption of Figure S5.

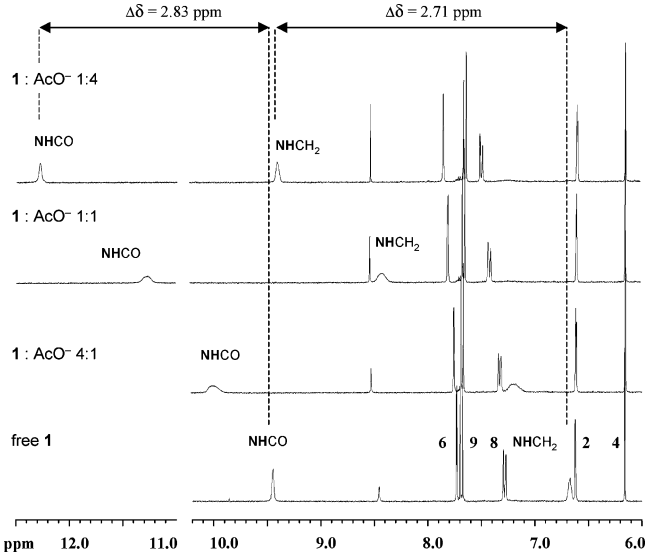

Figure 6. Selected spectra of a ^1H NMR titration of **1** with NBu_4AcO in DMSO-d_6. The Δ-shifts of the most important signals are indicated. For numbering, see Chart 1.

paragraphs. **1** shows strong interaction with AcO^- resulting in an easily discernible change of the color and a dramatic displacement of the urea NH-protons in the NMR spectra (Figure 6). As expected, both NH signals of **1** shift strongly downfield over the entire investigated range of compositions due to a hydrogen bonding-induced net deshielding.[76] The Δ-shifts, the chemical shift differences $\Delta\delta$ ($= \delta_{1/anion} - \delta_1$) of 2.83 and 2.71 ppm for NH−CO and NH−CH_2, respectively, demonstrate that both NHs are equally involved in the hydrogen bonding interaction. Apart from the downfield shifts of the NHs, only minor displacements are observed for the other protons of the molecule, indicating the absence of other strong intermolecular interactions between **1** and AcO^- ions. For comparison, the acetate affinity of the acetamide derivate **3** was also investigated. In contrast to **1**, only very minor chemically induced shifts $\Delta\delta$ were observed during a titration (Figure S1), indicating only weak interactions and a negligible tendency for hydrogen bond formation for this dye-anion pair. $\Delta\delta$ for the amide NH is only 0.38 ppm and the other proton signals of **3** are even less affected.

Being aware of the controversy that exists on the signaling of fluoride in organic solvents by sensor molecules with amido, urea, thiourea or pyrrole-type receptors, i.e., whether an actually

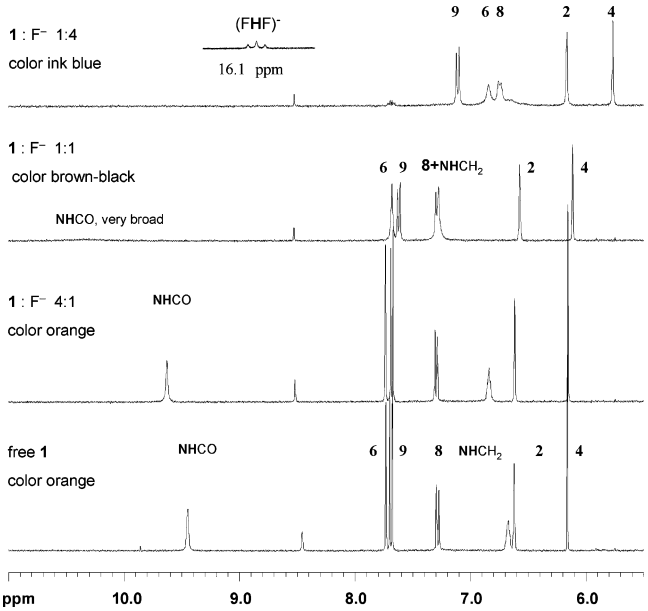

Figure 7. Selected spectra of a ^1H NMR titration of **1** with NEt_4F in DMSO-d_6. The Δ-shifts of the most important signals are indicated. For numbering, see Chart 1.

hydrogen-bonded complex is formed or whether fluoride deprotonates the ligand,[77] the responses of **1** and **3** upon addition of fluoride were also investigated by NMR spectroscopy. As can be deduced from Figure 7, **1** qualitatively shows the same characteristics as described before for **1**/AcO^- at low fluoride-to-probe ratios (Figure 7, lower middle, **1**: $F^- = 4{:}1$). However, in the further course of the titration, the NH proton resonances broaden considerably and have almost completely disappeared at equimolar ratios of anion and **1**. Simultaneously with the disappearance of the NH signals, a new 1:2:1 triplet signal at 16.1 ppm appears, which can be attributed to the bi-fluoride ion (FHF^-) with a coupling constant $^1J_{HF} \approx 120$ Hz.[78] The occurrence of this new species points to a deprotonation of either the urea group or of the solvent. There are indications of both. The strong high-field shift of all the phenoxazinone proton signals, indicating an overall change of the electron distribution in the chromophore, gives evidence to the deprotonation of the urea moiety. On the other hand, the ^{19}F NMR spectrum features a F−D−F signal in addition to the F−H−F signal. Similar observations were made during a titration of model compound **3** with F^-, the reaction occurring even at lower anion concentrations (Figure S2). Strong line broadening of the NH−CO signal and a color change from orange to brown is already found at **3**: F^- ratios of 4:1. At a 4-fold excess of fluoride, deportonation

(76) Hibbert, F.; Emsley, J. *Adv. Phys. Org. Chem.* **1990**, *26*, 255−379 and references therein.
(77) See, e.g., 13*p* or Black, C. B.; Andrioletti, B.; Try, A. C.; Ruiperez, C.; Sessler, J. L. *J. Am. Chem. Soc.* **1999**, *121*, 10438−10439. Sortino, S.; Conoci, S. *Chem. Phys. Lett.* **2000**, *323*, 389−392. Sun, S.-S.; Lees, A. J. *Chem. Commun.* **2000**, 1687−1688. Kim, S. K.; Yoon, J. *Chem. Commun.* **2002**, 770−771. Aldakov, D.; Anzenbacher, Jr., P. *Chem. Commun.* **2003**, 1394−1395. Unfortunately, many studies on molecular fluoride sensors that operate in organic solvents do not report on observations in the seldomly studied region of the ^1H NMR spectrum where the FHF^- species can be observed. For further discussions, see Tabata, M.; Kaneko, K.; Murakami, Y.; Hisaeda, Y.; Mimura, H. *Microchem. J.* **1994**, *49*, 136−144, Gunnlaugsson, T.; Kruger, P. E.; Jensen, P.; Pfeffer, F. M.; Hussey, G. M. *Tetrahedron Lett.* **2003**, *44*, 8909−8913, Lee, J. Y.; Cho, E. J.; Mukamel, S.; Nam, K. C. *J. Org. Chem.* **2004**, *69*, 943−950 and refs 12*e* and 13*q*.
(78) Shenderovich, I. G.; Limbach, H.-H.; Smirnov, S. N.; Tolstoy, P. M.; Denisov, G. S.; Golubev, N. S. *Phys. Chem. Chem. Phys.* **2002**, *4*, 5488−5497.

Chart 4. Deprotonation of 7-amido-phenoxazinones. The Calculated Absorption Maxima and Oscillator Strengths *f* for **3** Are Indicated (gas phase, obtained with ZINDO/S for the AM1-optimized geometries). For Comparison, the Absorption Maximum of **3** Shifts from 467 to 619 nm in a Titration with F^- in DMSO and Is Accompanied by a ca. 2.5-fold Increase in Molar Absorptivity, See Figure S5

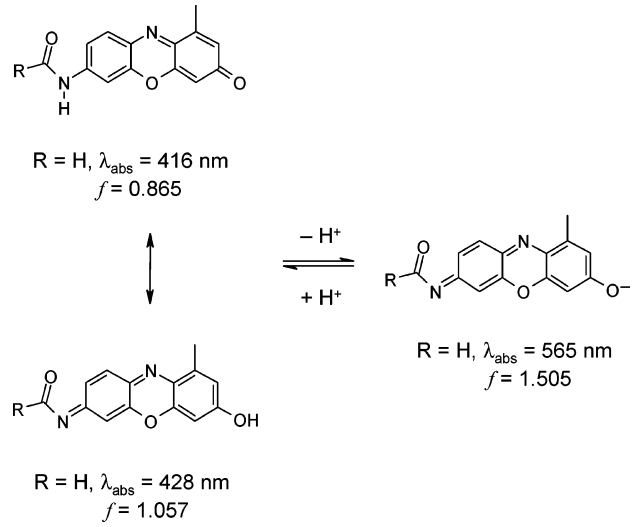

is complete. These NMR findings strongly support the unequivocally different chromo- and fluorogenic changes observed for acetate and fluoride in the optical spectroscopic studies (Figure 3). Apparently, when the 7-amido- or 7-urea-phenoxazinone skeleton is deprotonated, a charge redistribution takes place within the molecule according to the equilibrium outlined in Chart 4 and the resulting $\mathbf{1}^-$ and $\mathbf{3}^-$ show almost typical characteristics of asymmetric cyanine dyes. The fact that fluoride can lead to the deprotonation of H-acidic functional groups are not surprising, as the "naked" fluoride ion is highly basic in aprotic organic solvents such as DMSO.[79]

Step from 1 to 2. Returning to the carboxylate sensing abilities of **1**, exchange of the organic solvent DMSO for water leads to the well-known disqualification of such simple urea-based sensor molecules, i.e., **1** does not show any response to carboxylates at all under such realistic conditions.[80] On this background, we were interested to see how the thiourea analogue of **1** would qualify as a molecular sensor. Due to the increased acidity of the hydrogen bond donor sites in such a derivative, slightly higher binding constants can usually be expected for probes carrying this receptor.[27] Moreover, as has recently been shown by Teramae's and Kubo's groups,[13o,24b,e] a further increase in host−guest binding strength might be obtained when converting a thiourea-appended fluorescent sensor molecule into its isothiouronium derivative. However, whereas the synthesis of **2** could be accomplished, any attempts to prepare an isothiouronium-appended dye according to procedures described by Kubo et al.[13o] for 2-[(*S*-benzyl-*N*'-methyl-*N*-isothiouronio)-methylnaphthalene hexafluorophosphate or by Teramae et al.[24e] for *S*-(2-naphthylmethyl)-*N*,*N*'-dimethylisothiouronium bromide, were unsuccessful.[81]

(79) Liotta, C. L.; Harris, H. P. *J. Am. Chem. Soc.* **1974**, *96*, 2250−2252. Bordwell, F. G. *Acc. Chem. Res.* **1988**, *21*, 456−463. Christe, K. O.; Brooke Jenkins, H. D. *J. Am. Chem. Soc.* **2003**, *125*, 9457−9461.

(80) In fact, **1** does not respond to any analyte in water, including the now well-solvated fluoride ion.

Table 4. Spectral Data of **2** in Selected Solvents at 298 K

solvent	λ_{abs}(max) /nm	λ_{em}(max) /nm
H_2O	516	597
MeOH	484	592
DMSO	487	610
MeCN	466	584
acetone	470	586
CH_2Cl_2	458	578
Et_2O	465	571

Subjecting **2** to similar spectroscopic studies as described above led to the results summarized in Table 4. However, whereas for all the dyes and complexes of **1** reported above fluorescence excitation and absorption spectra match, this was not found to be the case for **2**. Additionally, the fluorescence quantum yields show a dependence on excitation wavelength, revealing a complicated behavior for this derivative already in the ground-state. In view of the unsuccessful synthetic attempts to prepare the isothiouronium dye and having in mind the ease of deprotonation of **1** and **3** in DMSO in the presence of fluoride, NMR spectroscopic and spectrophotometric studies with AcO^- and F^- were performed for **2** in analogy to those described above. As can be seen in Figure S3, the shifts in the NMR spectrum induced by acetate are even stronger than those found for **1**, and even a partial deprotonation is noticed in the absorption spectrum of **2** in the presence of this anion in DMSO (see Figure S6). Moreover, the presence of fluoride leads not only to broadened NH signals, but to an unspecific reduction of all the signals, most probably due to the decomposition of the compound (Figure S4). We tentatively assume that due to the strong phenoxazinone push−pull system, the thiourea moiety is too acidic to produce a straightfoward and robust spectroscopic behavior. Taking further into consideration that **2** deprotonates already with acetate, which suggests that the compound might also not be sufficiently stable or might not yield well-defined host−guest chemistry in other media, we refrained from carrying out any other complexation experiments and did not consider **2** any further for the development of a sensor material.[82]

Synthesis, Spectroscopic Properties, and Performance of the Sensor Materials

So far, the signaling features of acetate-enhanced fluorescence well within the visible spectral range established for **1** are very promising. However, its selectivity with respect to the target long-chain carboxylates and its performance—the failure to indicate any anion in water—are poor. To improve the two latter while maintaining the former, we invoked the strategy outlined above and linked an anchor-functionalized derivative of **1**, **TES1**, in a first step covalently to the surface of an easily modifiable solid support, the MCM-41 type UVM-7 material (Chart 5). On the basis of the experiments made by Ganschow et al.,[53c] the critical dependence of the spectroscopic performance

(81) No change in the reaction mixture occurred upon heating of **2** with benzyl bromide in dry EtOH at 60 °C under Ar atmosphere for several hours. Altering the conditions to heating **2** in anhydrous DMF with an excess of 5 equivalents of pentyl bromide under Ar atmosphere for more than 24 h did also not result in a success when following the advance of the reaction by TLC.

(82) DMSO solutions of **1** as well as neutral aqueous solutions of **1**, **M1**, and **M1Me**−DdO^- showed excellent stability over a testing period of 9 months. Furthermore, **M1Me** stored floating on water over that period of time also did not show any reduced performance.

Chart 5. Synthetic Scheme of the Preparation of the Hydrophilic and Hydrophobic Sensor Materials **M1** and **M1Me**. (a) Py, 80 °C; (b) UVM-7, Toluene:DMF (8:1), 80 °C; (c) HMDS, *n*-hexane, Room Temperature

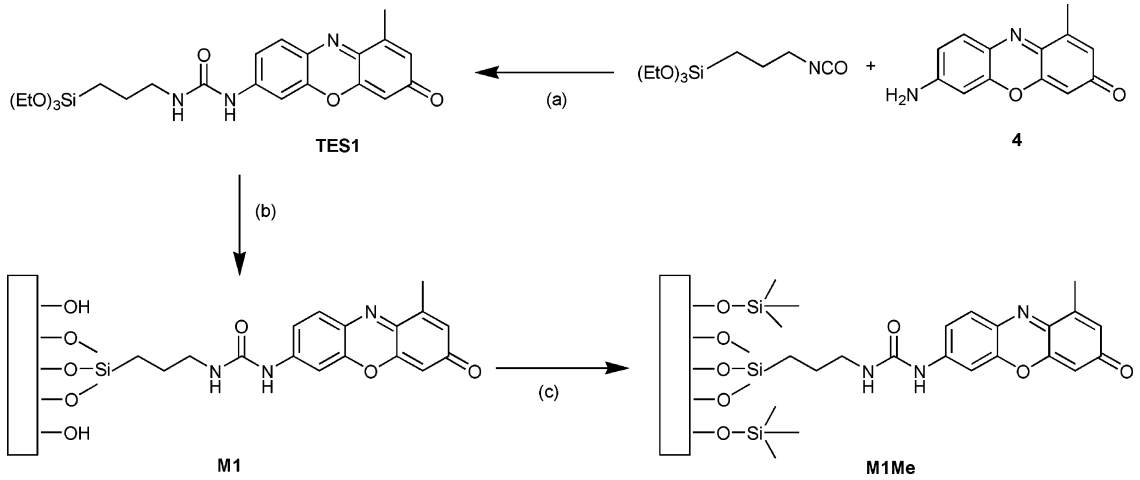

of such a hybrid material on interchromophore distances has to be considered in the material's design. The important factor here is that too high loadings of the chromophore could easily result in self-quenching. For instance, these researchers reported that 0.07 mmol of dye (a rhodamine derivative) per 2.4 g of TEOS (or 0.1 mmol of dye per g SiO_2) already entail a 50% decrease of the fluorescence signal. Transferring these data to interchromophoric distances, these studies revealed that a 50% decrease in the fluorescence intensity was observed with an average interchromophoric distance of ca. 6−7 nm in the rhodamine case.[53c] As we observed similar effects in previous studies with another UVM-7-phenoxazinone system,[83] we deliberately chose a lower chromophore functionalization ratio for the title materials. The optimum materials introduced here as **M1** and **M1Me** are functionalized with one sensor molecule every 13 nm, vide infra.

To introduce the second recognition element, the "hydrophobic pocket", to the sensor material, the remaining OH groups in **M1** were reacted with HMDS (1,1,1,3,3,3-hexamethyldisilazane), yielding the hydrophobic material **M1Me** (Chart 5). Characterization of the materials by XRD and N_2 adsorption−desorption techniques revealed that the typical features of a MCM-41 phase of the blank UVM-7 material are retained in both hybrids, suggesting that the structural ordering of the channels was not changed by the tandem functionalization (Figure S7). **M1Me** shows N_2 adsorption−desorption isotherms that are similar to those of the parent UVM-7 material (Figure 8). These are characterized by two adsorption steps (at intermediate and high P/P_0 values) related to the bimodal pore system. The first step corresponds to the nitrogen condensation inside the intra-nanoparticle mesopores (MCM-41 type, 2.4 nm) and the second one to the condensation inside the large interparticle pores (37.4 nm, textural porosity). Application of the BET model resulted in a value for the total specific surface of 1190 $m^2\ g^{-1}$. The inset of Figure 8 shows the pore size distribution.

Spectroscopic Properties of M1 and M1Me. UV/Vis spectrophotometry was employed to estimate the final dye loadings of the materials by comparison of the molar absorptivities of **1**, **M1** and **M1Me** in DMSO. As can be deduced from Figure 9, both materials are optically transparent as 0.1 mg mL^{-1} suspensions in DMSO. Furthermore, a comparison of the absorption spectra of **M1** and **M1Me** with that of **1** in Figure 3 suggests that the pores are entirely filled with the solvent and the well-solvated probes can freely move in the host. Apparently, a solvent with a high solvation ability such as DMSO largely levels out the influence of the differently polar

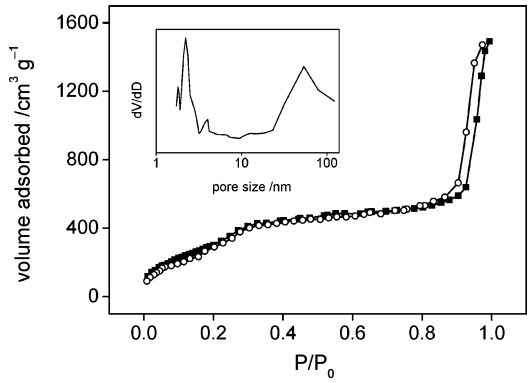

Figure 8. N_2 adsorption (squares) -desorption (circles) isotherms and pore size distributions (inset) of **M1Me**.

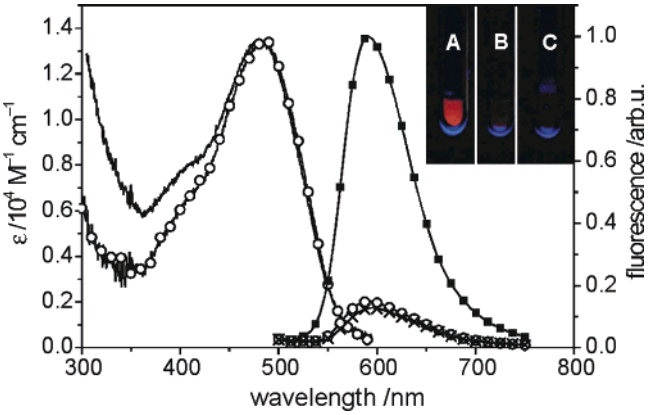

Figure 9. Absorption spectra of **M1** (circles) and **M1Me** (solid line) in DMSO, and emission spectra of **M1** in the absence (circles) and presence of DdO^- (crosses, virtually superimposed) as well as **M1Me** in the presence of DdO^- (squares) in water. The photograph visualizes the results: (**A**) **M1Me**−DdO^-, (**B**) **M1**, and (**C**) **M1**/DdO^- in water.

(83) Descalzo, A. B.; Martínez-Máñez, R.; Rurack, K.; Amorós, P. Manuscript in preparation.

Table 5. Steady-State Spectroscopic Data of **M1** and **M1Me** in Selected Media at 298 K

	solvent	λ_{abs}(max)/ nm	λ_{em}(max)/ nm	Φ_f
M1	H_2O	512	591	*a*
	DMSO	483	589	0.024
	dry powder[b]	n.d.[c]	587	n.d.[c]
M1Me	H_2O	*d*	*d*	*d*
	DMSO	481	594	0.026
	dry powder[b]	n.d.[c]	581	n.d.[c]

[a] Not determined because **M1** immediately settles, preventing the formation of a stable suspension as in DMSO. [b] From CLSM fluorescence measurements. [c] Not determined. [d] **M1Me** floats on aqueous solutions.

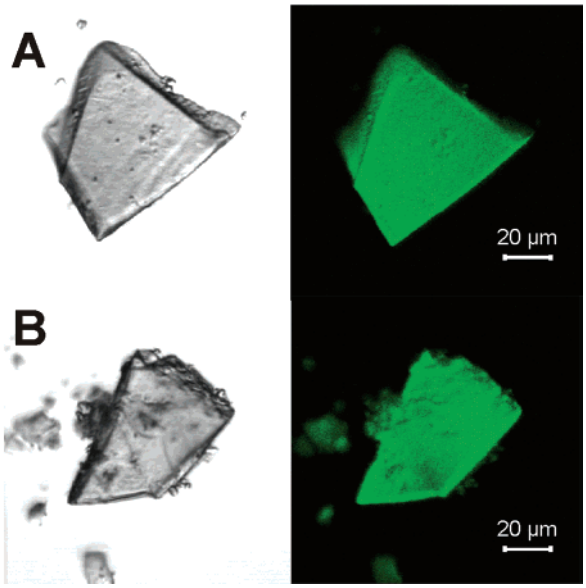

Figure 10. Typical confocal laser scanning microscopy (CLSM) images of **1**-loaded MCM-particles (**A**) **M1** and after re-functionalization of the inner surface (**B**) **M1Me** in transmitted light detection (left) and using the FITC fluorescence channel (right) of the confocal microscope.

MCM matrixes (cf. also the respective data in Tables 2 and 5). With the molar absorptivity of **1** in DMSO amounting to 13 460 cm^{-1} M^{-1} (Table 2), quantitative analysis of the absorption spectra measured for transparent suspensions of weighted **M1Me** samples in this solvent allowed to estimate the actual dye loadings. Following this procedure, a dye concentration of (1.21 $\pm$ 0.04) $\times$ 10^{-5} mmol mg^{-1} solid ($N = 8$) is found for **M1Me**. Taking into account the specific surface area, the coverage of active groups in **M1Me** is estimated to one **TES1** moiety per 165 nm^2 or one molecule every 13 nm. Using this value of the dye concentration of **M1Me**, an approximate functionalization of 4.9 mmol CH_3 g^{-1} solid is calculated for this material on the basis of the TG analysis results. Employing fluorescence microscopy, the macroscopic particle sizes could be determined to 40−80 μm edge length, having no geometrically defined shape (Figure 10). The fluorescence spectra measured for a single particle of the dry solids **M1** as well as **M1Me** shown in Figure 11 are in good agreement with the fluorescence features obtained for an arbitrary ensemble in the cuvette-based solution/suspension experiments in a conventional fluorometer (Figure 9).

Chromo- and Fluorogenic Anion Signaling Features of M1Me. Upon proceeding to aqueous media, the opposite polarities of both solids become obvious. Whereas hydrophilic

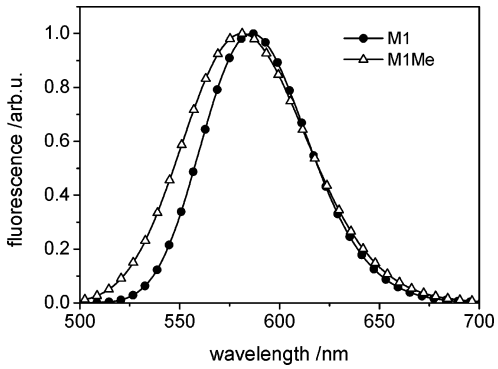

Figure 11. Normalized CLSM fluorescence of individual MCM particles **M1** and **M1Me**. Spectra were recorded with a channel range of 5 nm between 500 and 700 nm and 100 λ-steps.

M1 easily disperses in water, lipophilic **M1Me** repels the liquid (Table 5). The most impressive effects were obtained when adding solutions of various sodium carboxylates. Because the solvating ability of water is commonly too high for urea-carboxylate hydrogen bond-assisted recognition, **M1** remains entirely silent toward carboxylates (Figure 9). In contrast, **M1Me** responds to certain types of carboxylates. In a simple cuvette experiment, a positive reaction can easily be traced by the eye. If binding occurs, the solid rapidly sinks into the aqueous solution while at same time a change in color and a strong increase in the fluorescence is noticed (Figure 9). Moreover, Table 6 clearly reveals that **M1Me** now shows the desired selectivity for the target long-chain carboxylates. While such analytes as dodecanoate (DdO^-) or stearate (OdO^-) induce an analytically favorable color change from orange to pink accompanied by a remarkable increase in fluorescence (Figure 9), the sodium salts of the short- and medium-chain carboxylates (entries 1−5 in Table 6) as well as the aromatic, (poly)hydroxy, or polycarboxylic acids (entries 13−16 in Table 6) do not give any response. Apparently, only sufficiently lipophilic anions are taken up due to strong noncovalent interactions. However, a favorable effect of the hydrophobic nanoscopic pore system is not only observed in the modulation of the selectivity of **1**, but the whole ensemble shows an increased sensitivity. The apparent binding constants (adsorption constants) for the interaction of **M1Me** with DdO^-, TdO^-, *c*-OdO^- and *c*,*c*-OdO^- in water listed in Table 7 were determined by performing a Langmuir-type analysis of fluorescence titration data as plotted in Figure 12 for **M1Me**−DdO^- employing eq 1. The increase in K clearly illustrates the synergistic effects of hydrophobicity and hydrogen bonding.

$$I = I_L \frac{Kc}{1 + Kc};$$

$$c = \frac{-\left\{\frac{1}{K} + \frac{n_M}{V} - c_0\right\} + \sqrt{\left(\frac{1}{K} + \frac{n_M}{V} - c_0\right)^2 + \frac{4c_0}{K}}}{2} \quad (1)$$

Here, K is the adsorption constant (that accounts for the interaction between the carboxylate and the recognition centers anchored to the solid) and I and I_L are the observed intensities for a certain anion concentration and in the presence of an excess of anion (the limiting value), respectively. c_0 is the added salt (mol L^{-1}) and n_M the maximum amount of adsorbed anion in the monolayer (mol). (The formalism that lead to the deduction

Table 6. Responses and Cross-sensitivities of the Sensor Materials against Various Analytes in Aqueous Solution[a]

		M1		M1Me	
entry	species[b]	response[c]	*c*/mM	response[c]	*c*/mM
1	NBu_4^+ AcO^- [d]	−	7	−	30
2	Na^+ BuO^-	−	7	−	30
3	Na^+ HeO^-	−	7	−	30
4	Na^+ OcO^-	−	7	−	30
5	Na^+ DeO^-	−	7	(+)	30
6	Na^+ DdO^-	−	30	+	30
7	Na^+ TdO^-	−	7	+	30
8	Na^+ HdO^-	−	*e*	+	*e*
9	Na^+ OdO^-	−	*e*	+	*e*
10	Na^+ *c*-OdO^-	−	7	+	30
11	Na^+ *c,c*-OdO^-	−	7	+	30
12	K^+ *t*-OdO^- (pH 10.7)	*f*	*f*	+	*e,f*
13	Na^+ benzoate	−	7	−	30
14	Na^+ salicylate	−	7	−	30
15	Na^+ glucuronate	−	7	−	30
16	3 Na^+ citrate	−	7	−	30
17	NBu_4^+ $H_2PO_4^-$	−	20	−	30
18	2 K^+ HPO_4^{2-} (pH 8.4)	−	20	−	30
19	3 K^+ PO_4^{3-} (pH 13.0)	*g*	100	*g*	100
20	2 K^+ HPO_4^{2-}/ K^+ $H_2PO_4^-$ (pH 7.0)	−	20	−	100
21	NBu_4^+ Cl^-	−	100	−	100
22	NBu_4^+ HSO_4^-	−	20	−	30
23	NEt_4^+ I^-	−	10	−	10
24	NBu_4^+ Br^-	−	10	−	10
25	NBu_4^+ NO_3^-	−	20	−	30
26	NEt_4^+ F^-	−	10	−	10
27	K^+ HCO_3^- (pH 8.7)	−	20	−	30
28	2 K^+ CO_3^{2-} (pH 11.3)	−[h]	20	−	30
29	Na_2SO_4	−	20	−	30
30	$Fe(ClO_4)_3$	−	*1*	−	*1*
31	NaCl	−	100	−	100
32	K^+ $DdOPO_3H^-$ (pH 4.5)	*i*	*i*	+	*e*
33	2 K^+ $DdOPO_3^{2-}$ (pH 9.0)	−	7	−[j]	20
34	$(HdO)_2PO_2H$ [k]	*i*	*i*	−	*e*
35	Na^+ $Gly(TdO)_2Phos^-$	*i*	*i*	−	*e*
36	$Gly(DdO)_2PhosCho$	*i*	*i*	*l*	20
37	$Gly(DdO)_3$	*i*	*i*	−	*e*
38	Cholesterol	*i*	*i*	−	*e*
39	Na^+ $Chol^-$	−	7	−	30
40	Na^+ $DChol^-$	−	7	−	30
41	K^+ AMP^- (pH 6.9)	−	10	−	30
42	2 Na^+ ATP^{2-}	−	10	−	30

[a] Unless otherwise noted, the experiments were conducted in buffered (0.1 or 0.01 M phosphate buffer) or unbuffered aqueous solutions of pH 6.8 at 298 K. Unbuffered solutions were necessary in various cases where the dissolution of the analyte salt was hampered in the presence of the buffer salts. In general, the phosphate buffer had no effect on the signaling at both concentrations. [b] Key: AcO^- = acetate, BuO^- = butyrate, HeO^- = hexanoate (caproate), OcO^- = octanoate (caprylate), DeO^- = decanoate (caprate), DdO^- = dodecanoate (laurate), TdO^- = tetradecanoate (myristate), HdO^- = hexadecanoate (palmitate), OdO^- = octadecanoate (stearate), *c*-OdO^- = salt of ω9 (cis) monounsaturated C_{18} acid (oleate), *c,c*-OdO^- = salt of ω6 (cis,cis) diunsaturated C_{18} acid (linoleate), *t*-OdO^- = salt of ω9 (trans) monounsaturated C_{18} acid (elaidate), $Gly(TdO)_2Phos^-$ = 1,2-dimyristoyl-sn-glycero-3-phosphate, $Gly(DdO)_2PhosCho$ = 1,2-dididodecanoyl-sn-glycero-3-phosphatidylcholine, $Gly(DdO)_3$ = tridodecanoyl-sn-glycerol, $Chol^-$ = cholate, $Dchol^-$ = deoxycholate. [c] + = strong response, (+) = weak response, − = no response. [d] No counterion effects observed with NBu_4^+, NMe_4^+, Rb^+, K^+, Na^+ or Li^+ acetates. [e] As these compounds are not readily soluble or insoluble in bidistilled water or 0.1 M phosphate buffer at pH 7, they where directly added as solid; + indicates that the anion was taken up by **M1Me** in less than one minute and a positive response was observed; − indicates that even after keeping the mixture at 50 °C with frequent ultrasonic treatment, no effect was observed; the negative response persists after subsequent storage over 24 h at room temperature. [f] The salt dissolves only partially in water, causing a strong scattering background; a color change was not observed. [g] Dissolution of the solid at pH = 13.0. [h] Slight increase in fluorescence, most probably as a consequence of the beginning of silica dissolution. [i] As these salts are insoluble in water, testing the response of **M1** was not possible. [j] At pH = 9.0, a slow and time-dependent increase of the signals is found over several hours. [k] At pH 7 with K^+ HPO_4^{2-}/2 K^+ $H_2PO_4^-$ buffer. [l] The solid sinks into the water, but there is no change in color or fluorescence, most probably due to a "surfactant effect" of the phosphatidylcholine.

Table 7. Apparent Binding Constants (log*K)* for **M1Me** and Different Carboxylates in Water at 298 K

carboxylate[a]	log *K*[b]
DdO^-	2.52 ± 0.12
TdO^-	3.32 ± 0.08
c-OdO^-	4.320 ± 0.014
c,c-OdO^-	4.36 ± 0.14

[a] Anion key, see Table 6. [b] *K* were determined as the average of double separate experiments for every carboxylate.

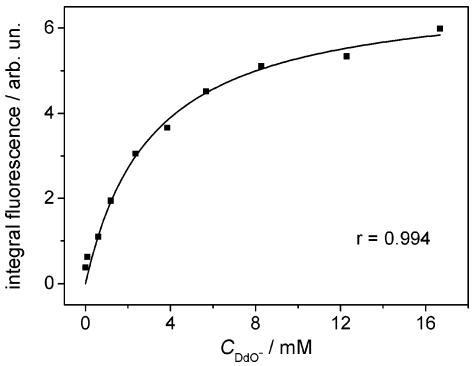

Figure 12. Titration curve for **M1Me** (1 mg in 2.5 mL water) with NaDdO in water, excitation at 475 nm.

of eq 1 is given in the Supporting Information.) Additionally, these binding constants are distinctly higher than that of **1**−AcO^- in DMSO, vide ante.[84] The studies reveal that limits of detection down to 10 μM can be obtained with **M1Me**. The sensing process itself is reversible and the response times are fast. Shaking cuvettes or capillaries with **M1Me**/DdO^-/water mixtures for 3 to 4 times after each step of analyte addition or each washing step was sufficient to reach a steady signal. The binding features of **M1Me** vs **M1** are also remarkable in their parallelism to the biological activity of certain alcohol dehydrogenases (ADHs). At millimolar concentrations, long-chain carboxylates enhance the activity of class III ADH up to 30-fold, with the size of the effect being positively related to the length of the anionic activator species.[85] Furthermore, among the different types of ADHs, the enzymatic activity toward ethanol is directly related to the hydrophilicity and cavity size of the substrate pocket of the enzyme. Thus, for class III ADH with the most hydophilic and largest pocket size, water competes most efficiently with ethanol and the aid of long-chain, more hydrophobic (co-)substrates is necessary to displace water and facilitate ethanol conversion. This effect is only found for carboxylates, not for their neutral fatty acid forms.[85]

The signaling features of **M1Me** are similar in all the long-chain cases, i.e., the above-mentioned color change and amplification of fluorescence. Again, microscopy experiments confirm the results obtained for an ensemble of the solids on a conventional fluorometer at the single particle level (Figure 13). To further elucidate whether the force predominantly determining the different binding constants—that vary for almost 2 orders of magnitude between the two extremes, DdO^- and *c,c*-OdO^-, vide ante—is the extraction effect of **M1Me** as the "hydrophobic

(84) Recently, Mizutani et al. found a comparable enhancement of the binding constant of a supramolecular host−guest system due to increased hydrophobic interaction for alkyl chain-appended porphyrin frameworks, Mizutani, T.; Kozake, K.; Wada, K.; Kitagawa, S. *Chem. Commun.* **2003**, 2918−2919.

(85) Moulis, J.-M.; Holmquist, B.; Vallee, B. L. *Biochemistry* **1991**, *30*, 5743−5749.

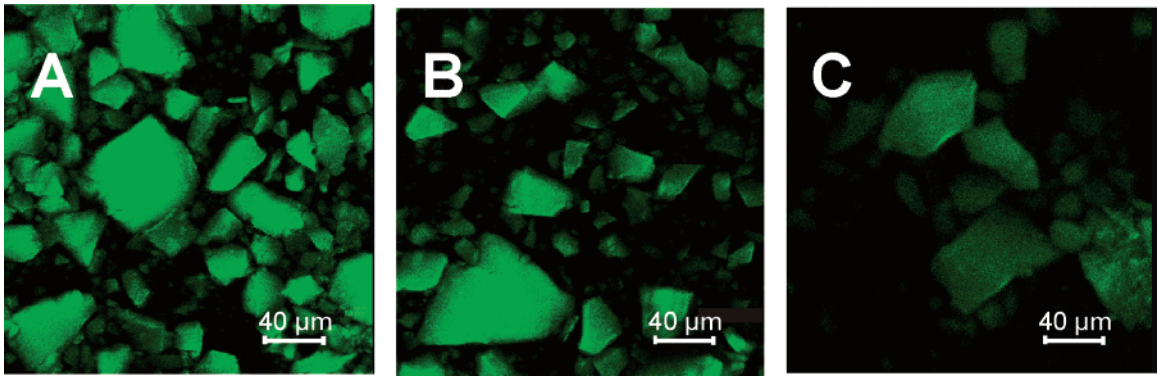

Figure 13. Increase in CLSM fluorescence signals after adding sodium dodecanoate (**A**) and oleate (**B**) to **M1Me** in aqueous solution. For comparison, the fluorescence image of **M1** in water (**C**) taken under identical experimental conditions is shown.

Table 8. Fluorescence Lifetime Data of **M1** and the Long-Chain Carboxylate complexes of **M1Me** in Water at 298 K

species[a]	$\langle\tau\rangle$/ps
M1	200 ± 80
M1Me−DeO$^-$	770 ± 320[b]
M1Me−DdO$^-$	850 ± 300
M1Me−TdO$^-$	830 ± 310
M1Me−HdO$^-$	760 ± 350[b]
M1Me−OdO$^-$	720 ± 370[b]
M1Me−*c*-OdO$^-$	860 ± 310
M1Me−*t*-OdO$^-$	610 ± 380[b]
M1Me−*c*,*c*-OdO$^-$	880 ± 270

[a] Anion key, see Table 6. [b] Overall center of a broad distribution with a bimodal character.

pocket" or a difference in the strength of the hydrogen bonding interaction between carboxylate and urea receptor site, time-resolved fluorescence experiments were carried out. If the actual hydrogen-bonding recognition event is responsible for the difference, then the fluorescence lifetimes of the complexes should also show distinctly different lifetimes. Before discussing the results given in Table 8, it is important to note that the fluorescence decays of **M1** as well as the various mixtures of **M1Me** and carboxylates in water do not show a strictly monoexponential behavior when discrete models are applied to deconvolute the data. Fitting the decay traces to discrete lifetimes, at least two species have to be employed to obtain satisfactory fits. This is not surprising as (i) the materials possess a bimodal porosity and (ii) presumably the individual sensor molecules are located in a large variety of slightly different microenvironments. Thus, in agreement with previous studies carried out by others as well as us on fluorescent dyes in confined media,[86] another model can be utilized to recover the decay kinetics, lifetime distribution analysis. This model is based on the assumption that in the ensemble the molecular emitter shows a quasi-continuous distribution of lifetimes or reaction rates.[87] The envelope of such a lifetime distribution function usually shows (at least) one peak that corresponds to the average lifetime $\langle\tau\rangle$ (or center of gravity) of a certain preferred species

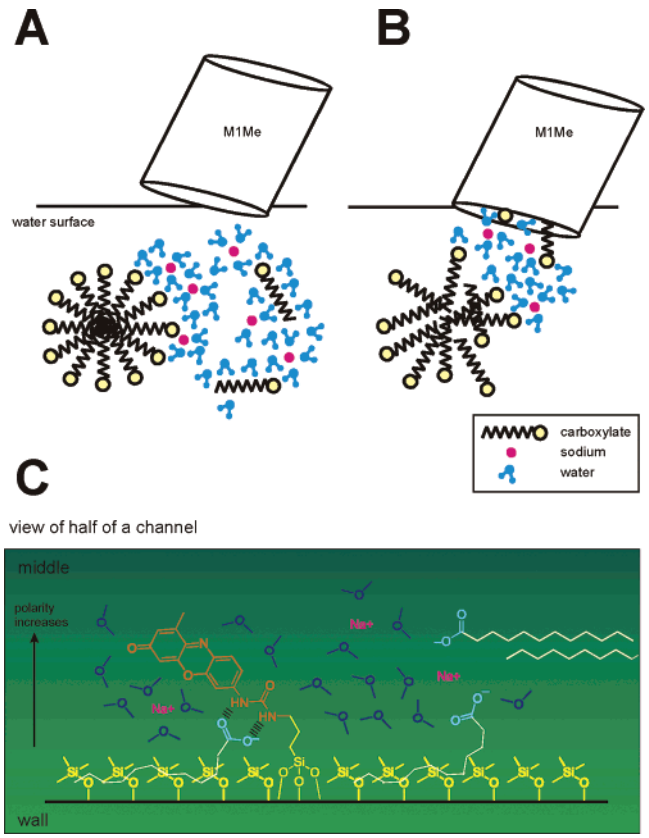

Figure 14. Schematic model of the response of **M1Me** toward long-chain carboxylates in aqueous solution. **A**: **M1Me** floats on the liquid's surface. **B**: Uptake of carboxylates, counterions and solvent molecules leads to a suspension of the hybrid in the solution. **C**: Hydrophobic forces "bind" the tail at the wall (mimicking the "pocket") while hydrogen bonding to the urea group generates the signal.

or environmental situation. The width of the function is then a measure for the microheterogeneity around the emitting species.

The lifetime data collected in Table 8 reveal that the chain length of the carboxylate has only a minor effect on this parameter. Accordingly, the distinctly different binding constants seem to be primarily determined by the forces governing the uptake of the guest and the strength of the hydrophobic interaction. On the basis of the results described so far, it is reasonable to assume that the recognition process of **M1Me** follows a model that is depicted in Figure 14. Whenever long-chain carboxylates are present in an aqueous solution, they can exist as monomers or from micellar-like objects (Figure 14A).

(86) (a) Ware, W. R. In *Photochemistry in Organized and Constrained Media*; Ramamurthy, V., Ed.; VCH: New York, 1991; pp 563−602. (b) Bright, F. V.; Catena, G. C.; Huang, J. *J. Am. Chem. Soc.* **1990**, *112*, 1343−1346. (c) Rurack, K.; Hoffmann, K.; Al-Soufi, W.; Resch-Genger, U. *J. Phys. Chem. B* **2002**, *106*, 9744−9752.

(87) Quasi-continuous refers to the finite number of single lifetimes that the software employed allows to fit to a given set of data. In our case, with the FLA900 program package allowing to include between 20 and 100 lifetimes, we obtained the best results with the maximum number of lifetimes. Representative examples of fits are given in Figure S9.

As these objects are not static but in a constant process of (partial) assembly and disassembly, the initially floating material can either extract monomeric species into its hydrophobic interior or can lead to the dissolution of the micelles (Figure 14B). Due to the size of the pores and for charge compensation, the long-chain carboxylates are not exclusively extracted, but counterions and solvent molecules also enter the pores. The final step of the simplified picture given in Figure 14C can be rationalized as the "binding" of the long-chain tail to the hydrophobic walls, whereby the polar headgroups stick to the outside. In this microscopic boundary layer of presumably reduced water content, the hydrogen bond-mediated binding reaction between the probe's receptor group and the carboxylate group is then facilitated and leads to signal generation. This hypothesis is further confirmed by one of the entries in Table 8 which needs special attention, **M1Me**−DeO$^-$. Although for this analyte, a sinking in of the solid material into the solution is hardly discernible and the weakness of the reaction did not allow to derive a binding constant from the fluorescence data, the time-resolved fluorescence experiments allowed to detect a second minor peak in the lifetime distribution function for high concentrations of the analyte, with the features listed in Table 8. The average lifetime of 770 ps of this ensemble of species suggests that although only a small fraction of DeO$^-$ is taken up by **M1Me**, binding and signaling occurs in a similar fashion. Apparently, the strength of the adsorption of the tail at the hydrophobic wall is the decisive parameter here.

Another somewhat unexpected result is the behavior found for the naturally only scarcely occurring trans analogue of oleate, elaidate (entry 12 in Table 6). The salt of this acid, which can usually be found in foodstuff only as a consequence of technological processing that involves the heating of fats, induces also an increase in average fluorescence lifetime. However, overall binding seems to be considerably weaker than for the other C-18 carboxylates, especially *c*-OdO$^-$ and *c*,*c*-OdO$^-$.[88] Any attempts to obtain a reliable binding constant failed due to the strong scattering of the data in the fluorometric experiments. At present, we cannot satisfactorily explain these findings, that might be related to the distinctive molecular behavior of monounsaturated fatty acids that also leads to differences in the interactions of *c*-OdO$^-$ and *t*-OdO$^-$ with fatty acid binding proteins.[89] These proteins are capable of discriminating among fatty acids on the basis of chain length and saturation state, most probably due to various interconnected forces that are at play in their "pockets", such as hydrophobic and/or hydrophilic sites as well as the residual content of water. Presently, however, the detailed molecular understanding of these processes is rather poor.[89]

Applicationary Aspects of the Performance of M1Me. Before the true qualification of **M1Me** as a potent sensor material can be assessed, it is important to know how the hybrid material behaves in the presence of potential interferences or competitors. The first question of course concerns the dissociation state of the target analytes. **M1Me** was designed as a sensor for the *salts* of long-chain fatty acids (LCFAs). Thus, it is important to remember that LCFAs are weak carboxylic acids with a pK_a of 4.75−5 and that at physiological pH, only 0.4% of the plasma fatty acids exist in the protonated form.[18b,90] Concerning small inorganic anions of biological and environmental relevance (entries 17−29 in Table 6), such species are neither recognized by **M1Me** nor by the material with a polar interior. In accordance with the results found for **1** and fluoride in water, this list includes F$^-$. Moreover, with respect to the cation sensor introduced by us in ref 41, no interference in water due to cation coordination at the carbonyl moiety was observed (entry 30 in Table 6). Fe^{3+} was tested here as this cation was found to coordinate strongest to the CO group in organic solvents in that work. Furthermore, it is important to note that no counterion effects on the analyte selectivity were observed when employing more lipohilic cations such as NEt_4^+ or NBu_4^+. Neither were the DdO$^-$ binding features noticeably changed, nor did the presence of such cations facilitate the recognition of short- or medium-chain carboxylates such as acetate or hexanoate. These results give further evidence to the fact that longer alkyl chains at the carboxylate are necessary to induce the binding reaction.[91]

Recalling the areas of analytical chemistry where the sensing of free carboxylates is most important,[15−22] blood plasma and food products are the most obvious ones.[92] Whereas FFA concentration in food can amount to 0.1% or more,[93] blood plasma levels can vary between 0.2 and 10.0 mM,[19a,94] depending on the health status of the organism and lying well within the applicable sensing range of **M1Me**, vide ante. Besides various of the small inorganic anions listed in Table 6 and with respect to the general preference of carboxylate binding sites for (di)hydrogenphosphates, the most prominent potentially interfering components would be neutral triglycerides, cholesterol, bile acids/salts, and the different classes of organic phosphates. We thus performed response studies with the compounds listed in entries 32−42 in Table 6. Among these species, only the mono-deprotonated form of a long-chain phosphate, dodecyl hydrogenphosphate (entry 32), gave a positive signal in a fashion similar to the long-chain carboxylates. Neither glycerophospholipids such as 1,2-dimyristoyl-sn-glycero-3-phosphate [Gly(TdO)$_2$Phos$^-$] or 1,2-didodecanoyl-sn-glycero-3-phosphatidylcholine [Gly(DdO)$_2$PhosCho] that are essential components of biological membranes,[95,96] nor bile salts such as cholate and deoxycholate, important for the fat metabolism in the liver,[96,97] induce a color change or significant increase in fluorescence. Additionally, bis long-chain substituted

(88) Overall binding refers to the macroscopically measurable apparent binding constant. At present, we cannot resolve which of the microscopic processes−uptake of the carboxylate, binding at the hydrophobic inner wall−accounts for this behavior.

(89) Woolf, T. B.; Tychko, M. *Biophys. J.* **1998**, *74*, 694−707.

(90) These pK_a values are characteristic for FFAs. When integrated in membranes, the pK_a of LCFAs can rise to 8.[18b] Concerning FFAs in extrenal applications, i.e., the relationship between solution pH and clinical irritancy for carboxylate-based personal washing products, the degree of dissociation can also be different, Murahata, R. I.; Aronson, M. P. *J. Soc. Cosmet. Chem.* **1994**, *45*, 239−246.

(91) Filter functions have recently been also found for vesicles and utilized by Teramae's group for the colorimetric sensing of lipophilic anions. These researchers placed the molecular sensor noncovalently in cationic micelles. Hayashita, T.; Onodera, T.; Kato, R.; Nishizawa, S.; Teramae, N. *Chem. Commun.* **2000**, 755−756.

(92) The average concentrations of FFAs in pristine as well as polluted aquifers (ca. 0.5−200 μg L^{-1})[14] are too low for **M1Me** to be employed for in situ monitoring. Preconcentration steps would be necessary.

(93) Innawong, B.; Mallikarjunan, P.; Marcy, J. E. *Lebensm.-Wiss. Technol.* **2004**, *37*, 35−41.

(94) Krebs, H. A. *Annu. Rev. Biochem.* **1950**, *19*, 409−430. Minda, H.; Larque, E.; Koletzko, B.; Decsi, T. *Eur. J. Nutr.* **2002**, *41*, 125−131.

(95) Tocanne, J. F.; Teissie, J. *Biochim. Biophys. Acta* **1990**, *1031*, 111−142.

(96) The ionization state of these types of compounds can strongly depend on concentration, temperature and interfacial pH. At physiological pH, in general, monovalent negatively charged species can be found.

(97) Igimi, H.; Carey, M. C. *J. Lipid Res.* **1980**, *21*, 72−90. Cabral, D. J.; Hamilton, J. A.; Small, D. M. *J. Lipid Res.* **1986**, *27*, 334−343.

organic phosphates such as $(HdO)_2PO_2^-$ are also silent, presumably lacking sufficiently free movement of the polar headgroup and possessing a less optimum arrangement of the headgroup's POO^- hydrogen-bonding motif. Moreover, the macroscopic results obtained in the experiments carried out with Gly-$(DdO)_2$PhosCho (see footnote *j* of Table 6) are a further indirect proof that the uptake of a surface-active compound alone is not sufficient to induce an analytical signal, but hydrogen-bonding to the urea moiety of the anchored probe is necessary to generate the spectroscopic response. This species solvates **M1Me**, but a color change or enhanced emission are not detected. If we further take into account that the only non-carboxylates that give a positive signal, free long-chain phosphatidates such as dodecyl hydrogenphosphate, are only locally generated as intermediates in the glycero(phospho)lipid synthesis cycles or in intracellular membrane transport situations in considerably low concentrations,[98] strong interferences on the performance of **M1Me** are not to be expected.

Conclusions

In conclusion, we presented a rational strategy for the development of a new hybrid optical sensor material. Structure−property relationships allowed to single out the optimal molecular sensor unit with spectroscopically advantageous properties. The signaling reaction implemented in the system i.e., a fatty carboxylate-induced chromogenic reaction accompanied by a strong enhancement of fluorescence emission in the 600 nm range clearly shows that optimization of the signaling unit is equally important to selectivity for obtaining powerful sensing devices. Apparently, structure−property relationships can present a rather facile, rapid, and low-cost alternative in the rational approximation of functional dye structures for sensing applications. Combination with solid-state and supramolecular design concepts in a "biomimetic" sense then enabled us to obtain a new sensing material with a remarkably enhanced performance (sensing properties in water) and tailor-made selectivity (long-chain vs short-chain carboxylates). The competition studies demonstrated that only the combined forces of actual hydrogen-bonding in the recognition process (inducing the red-shift) and noncovalent interactions, enabling the discrimination, lead to an active response. Due to its high flexibility, the present design allows a facile adaption to various analytes and harbors an enormous potential for the future development of optical signaling devices.

Concerning the target analytes of this paper, the anions of free fatty acids, we believe that **M1Me** is a promising candidate for future in-situ analytical applications. **M1Me** can potentially be employed with conventional or microfluorometric instrumentation, operating with visible-range light sources. The sensor material works in water, the recognition process is reversible, and the material is not very prone to counterion or electrolyte effects. Moreover, for many applications in FFA analysis, the limit of detection and dynamic working range are suitable.

Experimental Section

Synthesis. General Methods. NMR spectra were recorded in DMSO-d_6 (δ_{ref} DMSO 2.49 ppm) on a Varian Gemini 300 spectrometer. Anhydrous pyridine, toluene and dimethylformamide were purchased from Aldrich. **4** was synthesized by condensation of *N*,*N*′-dichloro-1,4-benzoquinonediimine[99] and orcinol in refluxing ethanol.[64] The preparation of **3** is described in the same publication,[64] and is achieved by reaction of **4** with acetic anhydride in pyridine at 0 °C. The synthesis of **5** has been previously reported by us.[41] **1**, **2**, and **TES1** were synthesized by addition of 30 mol of the corresponding isocyanate or isothiocyanate to one mole of **4** in anhydrous pyridine and heating of the mixture to 80 °C under Ar atmosphere. After 6 h, the pyridine was evaporated, and the crude residue was chromatographied on silica gel with CH_2Cl_2:EtOH (30:1). UVM-7 supports were prepared according to a previously described procedure.[63]

7-(*N*′-Butylureido)-1-methyl-3H-phenoxazin-3-one (1). 0.014 g (0.062 mmol) of **4** and 0.184 g (1.86 mmol) of butyl isocyanate in 2 mL pyridine yielded 0.011 g of a brilliant orange-reddish solid (55%). ^{1}H NMR (DMSO): $\delta = 0.90$ (t, 3H, CH_2CH_3, $J = 7.3$ Hz), 1.25−1.38 (m, 2H, $CH_2CH_2CH_3$), 1.39−1.48 (m, 2H, $CH_2CH_2CH_2$), 2.35 (s, 3H, ArCH_3), 3.08−3.15 (q, 2H, CH_2CH_2NH, $J = 5.8$ Hz), 6.18 (s, 1H, Ar*H*), 6.46 (t, 1H, CH_2NHCO, $J = 5.5$ Hz), 6.63 (s, 1H, Ar*H*), 7.27 (d, 1H, Ar*H*, $J = 8.8$ Hz), 7.70 (d, 1H, Ar*H*, $J = 8.8$ Hz), 7.73 (s, 1H, Ar*H*), 9.22 (s, 1H, CO*NH*Ar). Exact Mass EI mass spectrum (m/z = M*)* calcd for $C_{18}H_{19}N_3O_3$: 325.1426, found: 325.1437.

7-(*N*′-Butylthioureido)-1-methyl-3H-phenoxazin-3-one (2). 0.020 g (0.088 mmol) of **4** and 0.30 g (2.60 mmol) of butyl isothiocyanate in 2.0 mL pyridine yielded 0.018 g of a dark reddish solid (60%). ^{1}H NMR (DMSO): $\delta = 0.90$ (t, 3H, CH_2CH_3, $J = 6.9$ Hz), 1.29−1.39 (m, 2H, $CH_2CH_2CH_3$), 1.49−1.59 (m, 2H, $CH_2CH_2CH_2$), 2.34 (s, 3H, CH_3Ar), 3.40−3.50 (m, 2H, CH_2CH_2NH), 6.20 (s, 1H, Ar*H*), 6.66 (s, 1H, Ar*H*), 7.38 (d, 1H, Ar*H*, $J = 9.7$ Hz), 7.75 (d, 1H, Ar*H*, $J = 8.7$ Hz), 8.08 (s, 1H, Ar*H*), 8.28 (s broad, 1H, CH_2NHCS), 10.10 (s, 1H, CS*NH*Ar). Exact Mass EI mass spectrum (m/z = M*)* calcd for $C_{18}H_{19}N_3O_2S$: 341.1198, found: 341.1108.

Synthesis of 1-Methyl-7-[*N*′-(triethoxysilyl)propylureido)-3H-phenoxazin-3-one (TES1). 0.030 g (0.13 mmol) of **4** and 0.96 g (3.9 mmol) 3-(triethoxysilyl)propyl isocyanate in 3 mL pyridine yielded 0.039 g of an orange-reddish solid (62%). ^{1}H NMR: $\delta = 0.58$ (t, 2H, CH_2CH_2Si), 1.15 (t, 9H, CH_2CH_3), 1.46−1.55 (m, 2H, $CH_2CH_2CH_2$), 2.35 (s, 3H, CH_3Ar), 3.08 (q, 2H, CH_2CH_2NH), 3.73 (q, 6H, CH_3CH_2O), 6.16 (s, 1H, Ar*H*), 6.55 (t, 1H, CH_2NHCO), 6.63 (s, 1H, Ar*H*), 7.27 (d, 1H, Ar*H*), 7.70 (d, 1H, Ar*H*), 7.73 (s, 1H, Ar*H*), 9.29 (s, 1H, CO*NH*Ar). Exact Mass FAB mass spectrum *m*/*z* calcd for $C_{23}H_{32}N_3O_6$-Si, [M+H]: 474.2060 found: 474.2126.

Synthesis of M1. TES1 (0.036 g, 0.08 mmol) was dissolved in a mixture of 16 mL anhydrous toluene and 2 mL anhydrous DMF. After heating to 80 °C under argon atmosphere, UVM-7 (1.00 g) was added and the suspension was stirred for 24 h. The solid was filtered off and washed with toluene and CH_2Cl_2. To ensure the complete removal of the nonanchored dye, the solid was Soxhlet-extracted with ethanol for 6 h.

Synthesis of M1Me. Silylation of the **M1** material was carried out with hexamethyldisilazane (HMDS) under mild reaction conditions.[100] **M1** (0.4 g) was suspended in 15 mL *n*-hexane and 0.97 g (6.0 mmol) HMDS were added at room temperature under argon atmosphere. The suspension was stirred overnight and the solid was filtered off and exhaustively washed with *n*-hexane and CH_2Cl_2.

Characterization of the Materials. X-ray measurements were performed with a Seifert 3000TT diffractometer using Cu Kα radiation. TGAs for **M1** and **M1Me** samples were carried out with a TGA/SDTA 851e Metler Toledo, with a heating rate of 10 °C min^{-1} from 393 to 1273 K. For **M1**, a weight loss of 7.1% corresponding to solvents (T < 180 °C) and another weight loss of 7.8% due to the decomposition of the organic groups (180 °C < T < 680 °C) were recorded. Likewise, TGA of **M1Me** resulted in a rather similar decomposition curve, revealing weight losses of 1.4% corresponding to solvents and 9.7%

(98) Brindley, D. N.; Sturton, R. G. In *Phospholipids*; Hawthorne, J. N., Ansell, G. B., Eds.; Elsevier: Amsterdam, 1982; pp 179−213. Kooijman, E. E.; Chupin, V.; de Kruijff, B.; Burger, K. N. J. *Traffic* **2003**, *4*, 162−174.

(99) Willstätter, R.; Mayer, E. *Chem. Ber.* **1904**, *37*, 1494−1507.

(100) Anwander, R.; Nagl, I.; Widenmeyer, M.; Engelhardt, G.; Groeger, O.; Palm, C.; Röser, T. *J. Phys. Chem. B* **2000**, *104*, 3532−3544.

due to the decomposition of the organic groups. IR spectra (Figure S8) were recorded on a Jasco FT/IR-460 Plus, and N_2 adsorption−desorption isotherms were measured on a Micromeritics ASAP2010.

NMR Spectroscopy. NMR titration experiments were carried out with a Bruker 400 MHz Avance NMR spectrometer (c_{dye} = 2.5 mM, 250 mM NBu_4AcO or NEt_4F stock solutions, the solvent signal at 2.49 ppm vs TMS was used as secondary standard). The actual dye-to-anion ratio was determined from the ratio of the methyl group signals of both species after each titration step. To avoid any misinterpretations of the deprotonation results in the case of fluoride addition, pure NEt_4F was measured in DMSO and was found to give no signal. Only after addition of a drop of water, a much broader signal appeared in that region, being typical for FHF^- in the presence of water.

Absorption and Fluorescence Spectroscopy. Steady-state spectra were recorded on a Bruins Instruments Omega 10 spectrophotometer and a Spectronics Instruments 8100 spectrofluorometer. Titrations were performed on a Perkin-Elmer LS50B spectrofluorometer. All measurements were carried out at 298 ± 1 K with dilute solutions, and the fluorescence measurements were performed with a 90° standard geometry and polarizers set at 54.7° (emission) and 0° (excitation). The fluorescence quantum yields (Φ_f) were determined relative to DCM in methanol (Φ_f = 0.43 ± 0.08)[101] and all the fluorescence spectra presented here are corrected; for correction procedures see ref 102. The uncertainties of the fluorescence quantum yields were determined to ± 3% (for $\Phi_f > 0.2$), ± 6% (for $0.2 > \Phi_f > 0.02$), ± 10% (for $0.02 > \Phi_f > 5 \times 10^{-3}$), and ± 15% (for $5 \times 10^{-3} > \Phi_f$), respectively. Fluorescence lifetimes (τ_f) were measured with a unique laser impulse fluorometer with picosecond time resolution, the setup described by us in an earlier publication[103] having been modified with respect to the excitation source: the 80 fs pulses of a Ti:Sa laser (Spectra Physics Tsunami, pumped by a Spectra Physics Nd:YVO_4 laser Millennia Xs) were used to seed a regenerative amplifier (Spectra Physics Spitfire P-5K, pumped with a Spectra Physics Nd:YLF laser Evolution X) that runs at 5 kHz. The typically 90 fs long output pulses were fed into an OPA (Spectra Physics OPA-800-F−HGII) and used to generate the respective excitation light by frequency quadrupling the idler of the OPA. Fluorescence was collected at right angles (polarizer set at 54.7°; monochromator with spectral bandwidths of 4 and 12 nm) and the fluorescence decays were recorded with a modular single photon timing unit described in ref 103. While realizing typical instrumental response functions of 25−30 ps half-width, the time division was 4.88 ps channel^{-1} and the experimental accuracy amounted to ± 3 ps, respectively. The laser beam was attenuated using a double prism attenuator from LTB and typical excitation energies were in the nanowatt to microwatt range (average laser power). Other details on the characterization and calibration of the instrument can be found in refs 102, 103. The fluorescence lifetime profiles were analyzed with a PC using the software packages Global Unlimited V2.2 (Laboratory for Fluorescence Dynamics, University of Illinois) and FLA 900/Level 2 (Edinburgh Instruments; for lifetime distribution analysis of single decays). The goodness of the fit of the single decays as judged by reduced chi-squared (χ_R^2) and the autocorrelation function $C(j)$ of the residuals was always below $\chi_R^2 < 1.2$.

Confocal Laser Scanning Microscopy. The fluorescence of individual MCM particles were determined by an inverse confocal laser scanning microscope (CLSM TCS2, Leica, Germany) with a 10× objective (dry) with a numerical aperture of 0.3. The fluorescence images were taken using excitation by an Ar^+-laser and detection by the FITC channel (excitation 488 nm (25%); RSP 500; emission 500−650 nm, PMT voltage ca. 700 V).

Quantum Chemical Calculations. Geometry optimizations were performed employing the semiempirical AM1 method (gradient < 0.01) and transition energies and oscillator strengths were calculated on the basis of these ground-state geometries and 1SCF calculations with a CI of 8 by the ZINDO/S method (Ampac V6.55, Semichem, Inc.).[104]

Acknowledgment. Financial support from the Ministerio de Ciencia y Tecnología (MAT2003-08568-C03-02, REN2002-04237-C02-01) and from the Generalitat Valenciana (GRUPOS03/035) is gratefully acknowledged. We thank Capsulution NanoScience AG, Berlin for letting us use their CLSM setup.

Supporting Information Available: NMR results on **2** and **3**, spectrophotometric responses of **3** to fluoride and **2** to acetate, XRD and IR spectra of the materials, examples of lifetime distribution analyses, and deduction of eq 1 (PDF). This material is available free of charge via the Internet at http://pubs.acs.org.

JA045683N

(101) Drake, J. M.; Lesiecki, M. L.; Camaioni, D. M. *Chem. Phys. Lett.* **1985**, *113*, 530−534.
(102) Rurack, K.; Bricks, J. L.; Schulz, B.; Maus, M.; Reck, G.; Resch-Genger, U. *J. Phys. Chem. A* **2000**, *104*, 6171−6188.
(103) Resch, U.; Rurack, K. *Proc. SPIE-Int. Soc. Opt. Eng.* **1997**, *3105*, 96−103.
(104) Dewar, M. J. S.; Zoeblich, E. G.; Healy, E. F.; Stewart, J. P. P. *J. Am. Chem. Soc.* **1985**, *107*, 3902−3909. Zerner, M. C.; Karelson, M. M. *J. Phys. Chem.* **1992**, *96*, 6949−6957.